Materials Advances

ROYAL SOCIETY OF CHEMISTRY

REVIEW

View Article Online
View Journal | View Issue

Cite this: *Mater. Adv.*, 2021, 2, 5513

Recent advances in graphene quantum dot-based optical and electrochemical (bio)analytical sensors

Ashish Kalkal, [a] Sachin Kadian,[bc] Rangadhar Pradhan, *[d] Gaurav Manik [b] and Gopinath Packirisamy *[ad]

Since the day of their origin, the graphene quantum dots (GQDs) have been considered a predominant material for biosensing applications in view of their unique and exciting electronic, physicochemical and optical properties. By combining the quantum-confinement and edge effects of carbon dots with the graphene structure, GQDs have emerged as a wonder material. These photoluminescent QDs possess remarkable biocompatibility, high current density, fast electron mobility, high water solubility, good photochemical stability, and low cytotoxicity, thereby prevailing in the field of sensing. Moreover, the high electron-transfer and easy biomolecule-immobilization capabilities of GQDs make them suitable for developing efficient (bio)analytical sensors. In this direction, the review is proposed to enlighten the scope of GQDs in a variety of optical and electrochemical chemosensors as well as biosensors. Recent advancements pertaining to their synthesis methods, unique properties, and their regulation through heteroatom-doping and surface-functionalization strategies are discussed, along with the current challenges and future prospects.

Received 23rd March 2021,
Accepted 15th July 2021

DOI: 10.1039/d1ma00251a

rsc.li/materials-advances

[a] *Nanobiotechnology Laboratory, Department of Biosciences and Bioengineering, Indian Institute of Technology Roorkee, Roorkee 247667, Uttarakhand, India. E-mail: gopi@bt.iitr.ac.in, genegopi@gmail.com; Fax: +91-1332-273560; Tel: +91-1332-285650*
[b] *Department of Polymer and Process Engineering, Indian Institute of Technology Roorkee, Roorkee-247667, Uttarakhand, India*
[c] *Department of Electrical & Computer Engineering, University of Alberta, Edmonton, AB T6G 1H9, Canada*
[d] *Centre for Nanotechnology, Indian Institute of Technology Roorkee, Roorkee 247667, Uttarakhand, India. E-mail: rangadhar@gmail.com*

Ashish Kalkal

Mr Ashish Kalkal is pursuing his PhD at the Department of Biosciences and Bioengineering, Indian Institute of Technology Roorkee. He received his MTech in Biomedical Engineering from the National Institute of Technology Kurukshetra (2016) and BTech in Electronics and Communication Engineering from Kurukshetra University (2014). At present, he has filed two Indian patents, published six research articles, two book chapters and one review article in peer-reviewed international journals. He is actively engaged in the synthesis of novel nanomaterials (graphene quantum dots, metal nanoparticles, Ti_3C_2-MXene and nanohybrid) and development of optical/electrochemical biosensors, nanosensors and microsensors for biomedical applications.

Sachin Kadian

Mr Sachin Kadian is the SERB-Overseas visiting doctoral fellow at the University of Alberta, Canada and is pursuing his PhD in Polymer and Process Engineering at the Indian Institute of Technology Roorkee since December, 2016. He received his MTech in Biomedical Engineering from the National Institute of Technology, Kurukshetra in 2016 and his BTech in Electronics and Communication Engineering from the University Institute of Engineering and Technology, Kurukshetra, India in 2014. His current research interests include the synthesis and characterization of quantum dots (graphene, sulfur, carbon, perovskites, and zinc oxide), nanomaterials, nanocomposites and their applications in biosensors, energy storage, photovoltaics, chemo-sensors, bioimaging and antibacterial agents.

1. Introduction

The emergence of nanostructured materials has generated enormous research interest for biomedical, printing, and optoelectronic applications in view of their interesting optical, electronic, and physicochemical properties.[1–7] Over the past decade, these materials have been broadly utilized toward the fabrication of electrochemical and optical biosensors.[8–11] Among them, the newly emerging zero-dimensional derivative of graphene, widely regarded as graphene quantum dots (GQDs), has itself provided increased advancements over the past decade. GQDs are essentially a subset of fluorescent carbon dots (CDs) and consist of the graphene structure (single or multiple layers of graphene) irrespective of the dot's size.[12–16] Graphene is known for its exceptional set of tunable properties: high mechanical strength, high elasticity, thermal stability, large surface area, and good electrical conductivity.[17,18] However, compared with graphene, GQDs have the added advantages of higher aqueous solubility, a tunable bandgap, and ease of surface functionalization due to edge and quantum-confinement effects.[13,19,20] Additionally, GQDs have excellent biocompatibility and the existence of multiple functional groups (hydroxyl, carboxyl, carbonyl, or epoxide) on their surface, which act as active sites on the edges or the basal plane and thus offer unparalleled benefits in the fabrication of biosensing platforms.[21–23] GQDs can interact with various biomolecules and other substrates using these active sites through π–π, electrostatic and covalent interactions.[11,24,25] Apart from the mentioned structural, biocompatible, and functional properties, GQDs provide inherent photoluminescence (PL) along with the capability to regulate their properties during or after synthesis, making them the most prominent candidate amongst the carbon family. The PL properties of GQDs remain the most fascinating that help in the fabrication of optical biosensors for the direct investigation of numerous target analytes in multi-faceted biological matrices.[26]

Despite numerous interesting properties, the short fluorescence lifetime and relatively low quantum yield (QY) of GQDs hamper their commercial aspects in developing different biosensing platforms. To overcome these limitations, surface functionalization

Rangadhar Pradhan

Dr Rangadhar Pradhan obtained his MSc degree in Zoology from Utkal University, Bhubaneswar in 2003 and his MTech and PhD degrees from IIT Kharagpur in 2006 and 2013, respectively. He did his postdoctoral research at NTHU, Taiwan. Presently he is a postdoctoral fellow at IIT Roorkee. Dr Pradhan got an MHRD scholarship for pursuing his MTech as well as his PhD. He has filed two patents and published more than 15 international research papers. He has also published one book. He has been a reviewer for many prestigious international journals. His research area includes the development of micro- and nano-biosensors.

Gaurav Manik

Dr Gaurav Manik is currently serving as an Associate Professor in the Department of Polymer and Process Engineering at IIT Roorkee. He holds a PhD (IIT Bombay), MTech (IIT Kanpur) and BTech (HBTI Kanpur) in Chemical Engineering. Prior to joining IITR, he served extensively in industry (3M, Indo Gulf Fertilizers & Chem. Ltd, Classic Stripes Pvt. Ltd) and academia (BITS Pilani, BIET Jhansi). His research interests include molecular modeling and simulations of polymer materials; chemical process modeling and simulation; and the development of novel polymer composites and nanocomposites, coatings, sealants, adhesives, quantum dots and nanomaterials. He has ~100 research publications in international peer-reviewed SCI journals, patent applications, conferences and book chapters.

Gopinath Packirisamy

Dr P. Gopinath is the Professor in the Department of Biosciences and Bioengineering at the Indian Institute of Technology (IIT) Roorkee, India. He earned his PhD in Biotechnology from the Indian Institute of Technology Guwahati, India. He did his postdoctoral research at the University of Rochester Medical Center, New York, USA. Currently his research group in the nanobiotechnology laboratory at IIT Roorkee is working on the development of polymer-based nanocarriers for the delivery of various anticancer and imaging agents. His group is also exploring new avenues for synthesizing novel nanomaterials for biosensing applications. At present he has more than 115 research publications in the area of nanobiotechnology in high-impact-factor journals. He has filed nine patents and has done one technology transfer. He has been a reviewer and editorial board member for many international journals. He has received numerous prestigious awards for his scientific contributions in the area of biomedical nanotechnology.

and heteroatom doping have emerged as the main approaches, which can help in regulating the electronic and optical characteristics of GQDs.[27] These property regulations can be accomplished during or after the synthesis of GQDs. In this context, different top-down and bottom-up synthesis approaches such as physical grinding, hydrothermal methods, electrochemical methods, incomplete carbonization, thermal pyrolysis, microwave methods, *etc.*, have been employed for controlling the size, structure, and optical properties of nanomaterials, including GQDs.[18,28] For instance, surface functionalization of GQDs with amine groups has been found to be very advantageous to improve their electronic and optical properties. Similarly, the heteroatom doping through sulfur (S), phosphorus (P), nitrogen (N), boron (B), fluorine (F), chlorine (Cl), selenium (Se), silicon (Si), *etc.*, have also been reported a powerful strategy to regulate their properties.

Therefore, in this review, efforts have been made to provide several elaborated sections to apprise the readers with a broad view of the implications of GQDs in the development of optical and electrochemical (bio)analytical sensing platforms (Scheme 1). The first appended section describes the various top-down and bottom-up synthesis strategies exploited for the preparation of GQDs. The second section elaborates on the optical and electrochemical properties of GQDs. The third section discusses the regulation of the GQD properties through heteroatom-doping and surface-functionalization strategies. The fourth section outlines the current advancements in GQD-based optical, electrochemiluminescent, and electrochemical biosensors. Finally, future prospects and current challenges pertaining to GQDs are summarized.

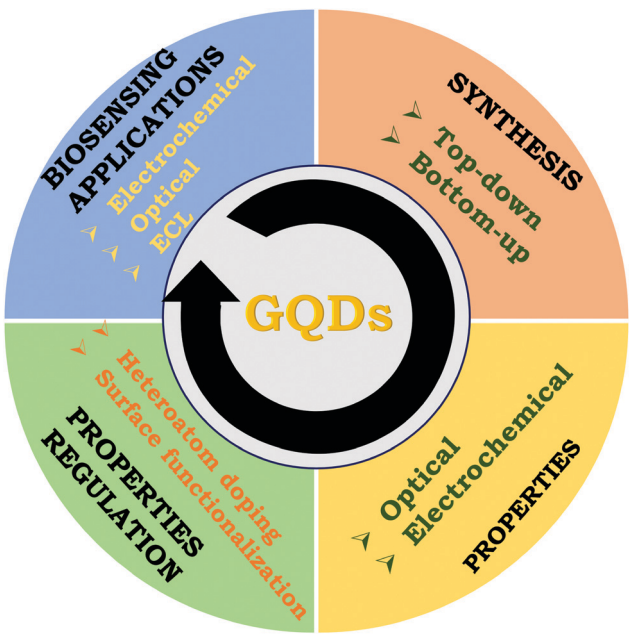

Scheme 1 Pictorial representation of various topics discussed in this review article: GQD synthesis strategies, properties as well as their regulation through heteroatom doping/surface functionalization, and (bio)analytical sensors (optical, electrochemiluminescence (ECL), electrochemical).

2. Synthesis strategies

The existing procedures for GQD synthesis can be structured into two broad aspects: top-down (the breakdown of bulk carbon materials) and bottom-down (the carbonization of small carbon-containing moieties) approaches.[29] Most synthetic processes under these two categories use commonly available precursors and are facile and inexpensive. These synthetic approaches and precursor materials play a pivotal role in regulating the properties of GQDs. The synthesis of GQDs in top-down approaches requires multifarious reaction stages, longer reaction times, and low production yields. On the other hand, bottom-up approaches use inexpensive organic precursors, require shorter reaction times, provide relatively higher production yields, and show ease of heteroatom doping during synthesis. In the following section, the recent progress in these two strategies has been delineated.

2.1 Top-down approaches

There are several processes for top-down approaches of GQD synthesis, such as oxygen cutting, physical grinding, hydrothermal/solvothermal methods, reductive cutting, electrochemical methods, *etc.* Oxygen cutting is one of the utmost used techniques, also known as chemical oxidation.[30–33] In this technique, bulk carbon materials (graphite, carbon black, charcoal (CC), carbon fiber (CF), graphene, graphene oxide (GO)) are typically cleaved to small fragments using sulfuric acid (H_2SO_4), nitric acid (HNO_3), or other oxidants. In this context, Ye *et al.* synthesized size-tunable GQDs using different types of coal as the starting material. Besides, the authors mentioned that coal is a better source compared with other sp^2 carbon allotropes for GQD synthesis because carbon within the coal structure can be easily cleaved *via* the oxidation process.[34] In another study, Dong *et al.* reported the chemical oxidation of CX-72 carbon black to synthesize single- and multi-layered GQDs.[35] Next, Zhang and co-workers demonstrated the synthesis of uniformly sized GQDs utilizing HNO_3 as a strong oxidant to remove oxygen-containing groups. The obtained GQDs were found to possess ample active sites and prevented the restacking of integral graphene nanosheets.[36] Maiti and colleagues described the preparation of GQDs having excitation-independent PL emission through the acidic exfoliation and oxidation of GO using perchloric acid. The obtained GQDs revealed a high QY of 14% with an average size of around 5.6 nm.[37] However, the safety of the oxygen-cutting procedure is not ascertained because of the use of strong oxidants, and the resultant extra substances can cause environmental pollution. To overcome this issue, Liu *et al.* reported (Fig. 1A) a novel acid-free method for obtaining GQDs from hydrogen peroxide (H_2O_2) and coal tar pitch (CTP) under ambient conditions.[38] Similarly, Lu *et al.*[39] manufactured GQDs with carbon black and H_2O_2 as the precursor and oxidant, respectively, providing GQDs with a diameter of 3.0–4.5 nm. The entire procedure takes around 90 min and the GQDs have the added advantages of high stability and reduced cytotoxicity. Following the particular study, Halder *et al.*[40] utilized GO as the precursor to synthesize GQDs in 2 hours through oxidation with H_2O_2 without the requirement of any post-purification procedure. Similar to

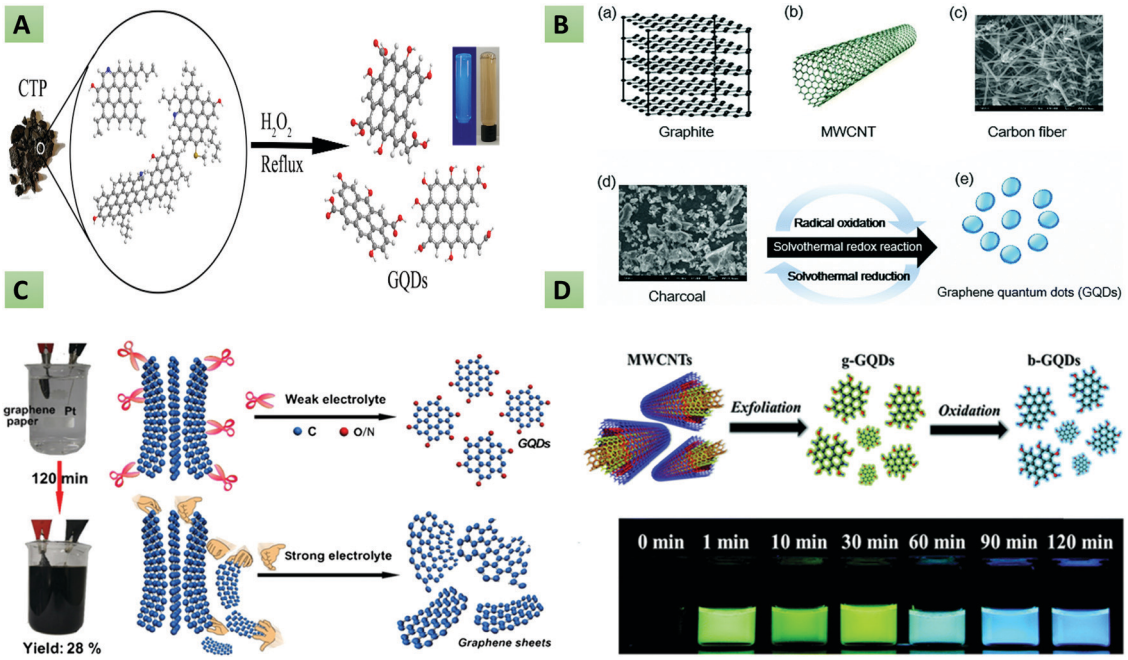

Fig. 1 Synthesis of GQDs *via* top-down approaches. (A) Oxygen cutting of coal tar pitch using H_2O_2 for obtaining blue fluorescent GQDs (republished from ref. 38, copyright 2018 MDPI). (B) Solvothermal reduction of graphite, MWCNT, and CF to GQDs (reproduced from ref. 53 with permission from the Royal Society of Chemistry). (C) Electrochemical exfoliation of graphene paper to GQDs (reprinted with permission from ref. 66, copyright 2018 American Chemical Society). (D) PLA process for the synthesis of blue- and green-colored GQDs from MWCNTs (reproduced from ref. 79 with permission from the PCCP owner societies).

oxygen cutting, reducing agents are also utilized to cleave the C–O bond in larger precursors. For instance, Giri and Gone demonstrated the synthetic mechanism of GQDs prepared using oxidized GO as the raw material.[41] Apart from this, it has been reported that the hydrothermal method is one of the simplest methods for manufacturing GQDs, which is also known as the solvothermal method.[42–45] In this context, Pu *et al.* first, in 2010, synthesized blue fluorescent ultrafine GQDs by cutting preoxidized graphene sheets using the hydrothermal method.[46] Later, the same group reported the synthesis of green fluorescent colloidal GQDs by improving the earlier method.[47] In recent times, numerous studies have reported the synthesis of GQDs *via* the hydrothermal method using graphene powder or GO as the precursor material.[48–51] Fan and coworkers described the large-scale synthesis of highly luminescent biocompatible and surface-functionalized GQDs *via* an environmentally friendly, low-cost, and facile hydrothermal method. The authors mentioned that GQDs, despite their remarkable optical properties, lack targeted specificity, restricting their biomedical application. In line with this, GQDs were surface-functionalized with polyethyleneimine (PEI) and then conjugated to (3-carboxyl) phenyl bromide phosphine (TPP) through amide linkage for their utilization in targeted bioimaging.[52] Shin *et al.* described (Fig. 1B) the solvothermal synthesis of GQDs utilizing CF, CC, graphite, and multiwalled carbon nanotubes (MWCNTs) as raw precursors.[53] Wu and their team reported the production of tunable PL emission GQDs *via* the hydrothermal treatment of ammonia (NH_3) and nanosized GO. It was mentioned that by varying the concentration of NH_3 in solution, the PL emission wavelength could be easily tuned.[54] Luo *et al.* demonstrated the hydrothermal treatment of GO and GQDs for modifying the electrochemical properties by incorporating GQDs into a three-dimensional graphene framework. The resultant nanohybrid exhibited increased supercapacitance owing to larger surface area and superior conductivity with the incorporation of GQDs.[55] In the hydrothermal/solvothermal method, the principle followed is to cause disruption of the bonds between graphene or GO sheets to produce GQDs at high pressure and temperature.[56–58] The experimental setup is eco-friendly, easy, cost-effective, and without the use of harsh oxidants. This particular technique has been successfully utilized in several biomedical sensors for the synthesis of highly fluorescent and biocompatible GQDs.[33,59,60] However, because of high applied temperature, pressure, and longer reaction time, there are several safety issues associated with this technique. In another method, Gao *et al.* reported three different kinds of GQDs, namely, pristine GQDs (PGQDs) from natural graphite, expanded GQDs (EGQDs) from expanded graphite, and GO quantum dots (GOQDs) from GO in a supercritical CO_2/H_2O medium aided by ultrasonic exfoliation.[61] This is a unique procedure aided by ultrasound wherein millions of bubbles created in the carbon or graphene sheet generate a mechanical force that destroy the carbon bonds inside, leading to the formation of the GQDs. The investigational consequences have demonstrated that this technique can provide an alternative green route as this is an eco-friendly, cost-effective, and quick synthesis method for GQDs, which may also be scaled up easily. In another article, Lu *et al.* described the synthesis of defect-controlled GQDs *via* an ultrasonic-assisted liquid-phase exfoliation strategy. In this method, nano-graphite and acetylene black were used to provide low-defect GQDs and high-defect GQDs, respectively.

The resultant GQDs were utilized as a potential fluorescent nanoprobes for bioimaging application in view of their controllable fluorescent performance, excellent biocompatibility and high water dispersibility.[62] Zhou *et al.* described the preparation of carboxyl GQDs using Fenton's reagent ($Fe^{2+}/Fe^{3+}/H_2O_2$) and GO under UV irradiation. This method was found to be suitable for the mass-scale production of GQDs.[63] Similarly, in another method, Lin *et al.* reported the high-yield synthesis of GQDs through the disintegration and exfoliation of MWCNTs and graphite flakes.[64] Another important method for GQD synthesis is electrochemical exfoliation, which is advantageous in some aspects compared with previously discussed methods. For instance, this method requires neither the use of strong acid nor conditions of high temperature and pressure. Besides, the method provides the benefit of cost-effectiveness and being environmentally friendly.[65] In this context, Hung and coworkers reported (Fig. 1C) the weak-electrolyte-based electrochemical synthesis of GQDs from graphene paper having a size from 3 to 8 nm.[66] Similarly, Li and their team synthesized P-doped GQDs through the electrochemical exfoliation of carbon electrodes.[67,68] Recently, Kalita *et al.* described the room-temperature synthesis of GQDs from GO utilizing the widely known three-electrode setup (working, counter, and reference electrodes) with 3 mM lithium perchlorate ($LiClO_4$) in propylene carbonate as the electrolyte. It was mentioned that the size of the GQDs can be regulated by optimizing different parameters *viz.* the supporting electrolyte concentration, the oxidation/reduction time and the applied voltage.[69] Ahirwar and coworkers demonstrated an electrochemical exfoliation route for the preparation of tunable GQDs wherein sodium hydroxide (NaOH) along with citric acid (CA) in water and graphite rods were utilized as the electrolyte and electrode, respectively. By keeping the concentration of CA fixed and varying the NaOH concentration, four types of GQDs (GQD1–GQD4) with tunable oxygen functional groups were obtained.[70] Yan and their team described an industrially promising, fast, and environmentally friendly electrochemical-exfoliation method for the production of functionalized GQDs using an ionic liquid (IL) and CF as the starting materials.[71] This procedure is also applicable to several other weak electrolytes and other anode precursors to create different kinds of GQDs. The drawbacks associated with the process include the tedious pretreatment of raw ingredients and the longer time duration involved in the purification of the GQDs. Additionally, the relatively low QY of the process makes it difficult to attain the large-scale synthesis of GQDs. Further, Yan *et al.* described the solution-processed synthesis of black GQDs having a uniform size for solar-cell applications.[72] Similarly, the synthesis of colloidal stable GQDs with desirable structures and sizes has been reported *via* a solubilization strategy by Yan and co-workers.[73] Apart from the above-mentioned techniques, some other popular techniques are chemical vapor deposition (CVD)[74] and the pulsed laser ablation (PLA) method.[75,76] Deka *et al.* reported highly stable hydrophobic GQDs using CVD that differentiated between aromatic and non-aromatic amino acids without any post-functionalization.[77] Kumar *et al.* described the fast, environmentally friendly, and simple synthesis of heteroatom-doped GQDs on copper foil employing the CVD technique and using chitosan as the starting material.[78] The PLA method was introduced in order to find a clean and novel way of synthesizing GQDs. In this context, Santiago *et al.* reported (Fig. 1D) the synthesis of green- and blue-colored GQDs utilizing carboxyl-modified MWCNTs as the precursor by regulating the time of the PLA process.[79] In a similar manner, the same group described the preparation of N-doped GQDs employing the PLA technique and using diethylenetriamine (DETA) as the starting material.[80] More recently, Kang *et al.* demonstrated the production of S-doped GQDs *via* the PLA method to tune the optoelectronic properties. Besides, it was observed that, compared with chemical methods, the PLA method provides more efficient doping of the carbon framework with S atoms.[81]

2.2 Bottom-up approaches

These methods generally utilize small molecules like amino acids or small sugar molecules as the starting material for GQD synthesis. These approaches primarily include cage opening, incomplete carbonization, thermal pyrolysis, microwave, and hydrothermal processes. For example, Gu *et al.* reported (Fig. 2A) the IR-assisted process for the preparation of N and S co-doped GQDs (N,S-GQDs) and N-doped GQDs (N-GQDs) utilizing CA, ammonium sulphate, and urea as precursors.[82] Chua and co-workers demonstrated the alteration of C_{60} into photoluminescent GQDs *via* a cage-opening procedure using concentrated H_2SO_4, sodium nitrate, and potassium permanganate.[83] Over the past decade, several studies have reported the synthesis of GQDs *via* carbonization or the pyrolysis method.[18,20,27,84–88] In line with this, first, Dong *et al.* tuned the carbonization degree of the carbon precursor (*i.e.*, CA) for the preparation of blue fluorescent GQDs (Fig. 2B).[89] The method has been reported as a cost-effective and green procedure that is used substantially to produce high-yield GQDs. The principle involved is to dehydrate organic biomolecules and then subject them to carbonization. The process involves hydrothermal reaction to dehydrate carbon bonds, followed by the interfacing of hydrogen bonds of one carbon-containing molecule to adjacent one forming water molecule and final interfacing with covalent bonds to form GQDs.[90–92] Next, Qu and colleagues demonstrated a hydrothermal route to prepare N-GQDs and N,S-GQDs using CA, urea, and thiourea as the source of C, N, and S, respectively.[93] Further, Zhang *et al.* prepared blue luminescent GQDs using aspartic acid as the raw precursor through a one-pot pyrolysis method.[94] Similarly, another group described the synthesis of N,S-GQDs *via* carbonization of CA and L-cystine.[95]

Likewise, the synthesis of sulphur-doped GQDs has been reported by Kadian *et al.* using CA and 3-mercaptopropionic acid (MPA) as raw precursors.[20] Liu and team described the pyrolysis of hexa-*peri*-hexabenzocoronene (Fig. 2C) into multi-color photoluminescent GQDs.[96] Recently, Gu *et al.* described the preparation of N-doped GQDs with tunable optical properties *via* infrared carbonization by using CA and urea as the starting materials.[98] Lee and co-workers demonstrated the production of the finest GQDs with fewer impurities and high crystallinity *via*

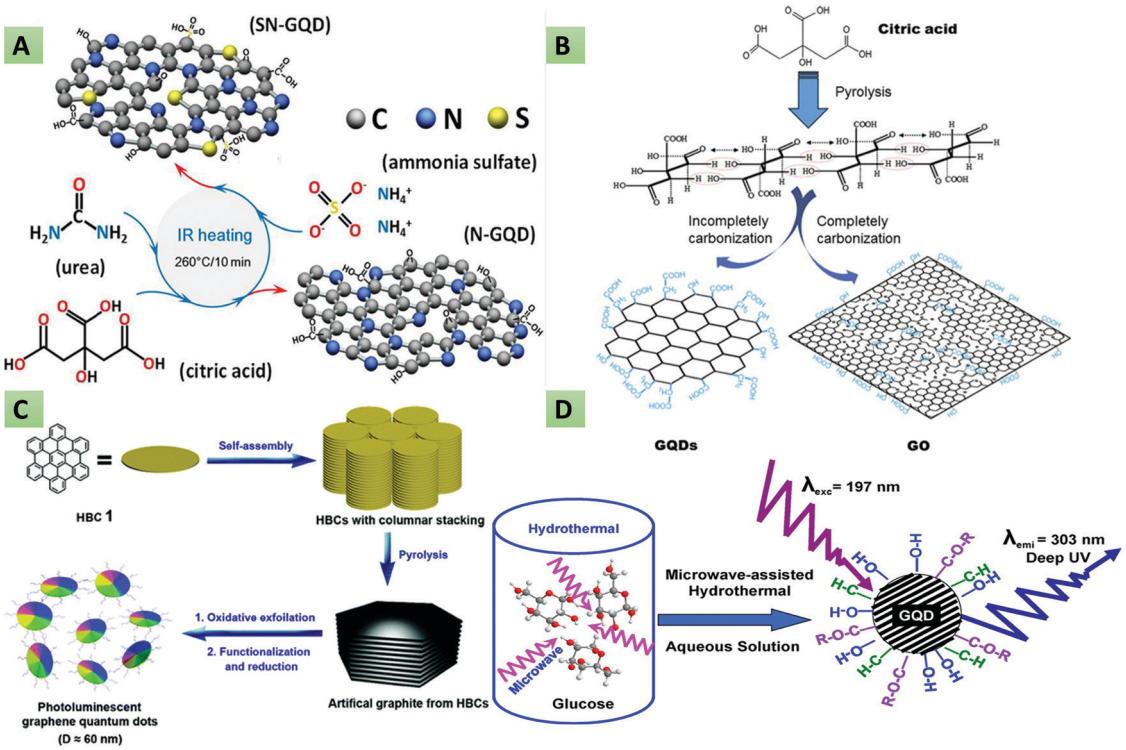

Fig. 2 Synthesis of GQDs *via* bottom-up approaches. (A) IR-assisted method for the synthesis of N-GQDs and N,S-GQDs using CA, ammonium sulphate, and urea as precursors (reproduced with permission from ref. 82, copyright 2019 American Chemical Society). (B) Carbonization of CA to provide blue fluorescent GQDs (reproduced with permission from ref. 89, copyright 2012 Elsevier B.V.). (C) Pyrolysis of hexa-*peri*-hexabenzocoronene into photoluminescent GQDs (reproduced with permission from ref. 96, copyright 2011 American Chemical Society). (D) Microwave-assisted hydrothermal synthesis (reproduced with permission from ref. 97, copyright 2012 American Chemical Society).

the hydrogen-assisted pyrolysis of silicon carbide.[99] Ping and their team synthesized D-penicillamine and pentaethylenehexamine (PEHA) co-functionalized GQDs *via* two-step pyrolysis using CA as the carbon source. The resultant GQDs offered a high QY (90.91%) and were used for the selective detection of glutathione (GSH) and mercury ions (Hg^{2+}).[100] More recently, Kalkal *et al.* reported amine-functionalized and N-doped GQDs *via* the hydrothermal carbonization of DETA and CA.[27] Hong and co-workers executed the thermal pyrolysis of trisodium citrate ($Na_3C_6H_5O_7$) at 200 °C for 4 min for the synthesis of monolayer GQDs having an ultra-small lateral size (1.3 ± 0.5 nm). The formation of GQDs was shown by the color change of $Na_3C_6H_5O_7$ from white to deep brown.[101] Li *et al.* described the preparation of carboxyl GQDs *via* the pyrolysis of CA and sodium chloroacetate under strongly basic conditions. The resultant GQDs were functionalized with folic acid for utilization in targeted photothermal therapy.[102] The use of these methods (thermal pyrolysis and hydro/solvothermal methods) is pretty challenging since they exhibit a change in reactor temperature, thereby providing uncontrolled size and structure.[18] To overcome these issues, microwave-assisted bottom-up synthesis has gained increased interest in view of its various benefits such as high yield, energy saving, reproducibility, low impurity and short reaction time.[94,103–106] From this perspective, Tang *et al.* reported a microwave-assisted synthetic method wherein glucose solution was irradiated with microwaves in an NH_3 environment (Fig. 2D). Besides, the authors mentioned that the optical properties of the as-synthesized GQDs could be regulated *via* the microwave reaction time and power.[97] In this method, Kumawat *et al.* demonstrated the preparation of self-assembled GQDs by employing the microwave-assisted one-pot method using grape seed extract as the starting carbon source. Owing to their remarkable optical properties, these GQDs were used for photoluminescent sensing, nucleus imaging, and cell proliferation applications.[107] Cardenas *et al.* utilized low-cost organic precursors (glucose and urea) in the presence of phosphoric acid toward the production of porous GQDs architecture *via* microwave-assisted synthesis.[108] Similarly, Yao *et al.* used glucose and ethylene glycol as the precursors in their bottom-up microwave-assisted technique for the synthesis of stable GQDs.[109] The microwave procedure has shortened the reaction time considerably. Moreover, this technique enables doping of the GQDs with numerous elements, which can play an essential role in drug delivery, cancer detection, and environmental analyte sensing *via* multicolor visible/near-infrared (NIR) fluorescence imaging. In line with this, Hasan and co-workers reported the facile microwave-assisted production of N,S-GQDs, and N-GQDs utilizing thiourea and glucosamine as precursors.[91] The as-synthesized GQDs showed varying optical characteristics in both the visible and NIR ranges. Pham and co-workers introduced the ultra-fast (within 5 min) synthesis of N-doped GQDs *via* a microwave method that uses CA and urea as the carbon and

Table 1 Summary of synthesis strategies of GQDs along with different characteristics

Method	Technique	Carbon source	Advantage	Disadvantage	Time (h)	Quantum yield (%)	Size (nm)	Ref.
Top-down	Oxygen cutting	Bituminous-coal	High stability	Lengthy process	1.5–2	51	2.9	34
		Carbon black	Cost-effective precursors	Require strong oxidants		2.29	18	35
						4.04	15	
	Hydrothermal	Oxidized GO	Simple and facile method	Lengthy process	12–24	—	2–5	41
		Graphene sheets	Cost-effective Environmentally friendly Narrow size distribution	Safety issue	15–20	6.9	10	46
	Solvothermal	CF, C, G, MWCNTs	Simple and facile method Eco-friendly	Lengthy process Low QY	10	0.05–0.31	2–8	53
	Ultrasound-assisted exfoliation	Graphite	Low cost High quality	Low yield Lengthy process to obtain precursors	2	1.86	2–4	61
	Electrochemical	Graphite	High QY Narrow size distribution	Tedious pretreatment of raw ingredients Longer time duration	8.5	14	5–10	111
	Pulsed laser ablation		One step Minimal experimental set-up Good reproducibility Shorter synthesis time	Costly	0.08–0.6	7–11	2–5	112
Bottom-up	Cage opening	C_{60}	Smaller size distribution	Lengthy process	20–24	—	2–3	83
	Carbonization. Thermal pyrolysis	CA	Easy and cost-effective method Controllable size and morphology Small reaction time	Limited precursors	0.5	9	15	89
	Hydrothermal	CA + DETA	High QY Narrow size distribution	Lengthy process	5	76.8	3	27
	Microwave-assisted hydrothermal	Glucosamine HCl and thiourea	One step Eco friendly High QY Smaller synthesis time	—	0.6	22–60	4–5	113

N dopants, respectively.[110] In another study, Li *et al.* described the scalable, superfast and simple preparation of single-crystalline and yellow fluorescent N-doped GQDs *via* the microwave strategy using 1,3,6-trinitropyrene as the starting material.[106]

In all, GQDs can be synthesized using both the bottom-up and top-down approaches. Table 1 summarizes the different synthesis strategies along with their different characteristics, advantages, and disadvantages. The vital benefits of the top-down strategies are the economics of scale, simplicity of the process, and plentiful availability of the raw materials. By contrast, the low production yield, usage of strong acids during synthesis, and longer reaction times hamper mass-scale production. Comparatively, hydrothermal/solvothermal methods are extensively utilized among several top-down strategies. Conversely, the bottom-up strategies are beneficial for synthesizing *in situ* functionalized, doped, and size-controllable GQDs with shorter reaction times. Microwave-assisted hydrothermal preparation is stated to be an environmentally friendly, quick, and in-expensive process for high-quality GQD synthesis *via* bottom-up approaches.

3. Optical and electrochemical properties of GQDs

3.1 Optical properties

GQDs have a high optical absorption when irradiated with UV light, producing different colored fluorescence (red, yellow, green, blue, *etc.*).[114,115] The PL emission spectrum can be excitation-independent (Fig. 3A) (*i.e.*, no shift in the emission peak with varying the excitation wavelength), which occurs due to the uniformity of surface states and the size of sp^2 clusters[89,116] or the excitation-dependent (a shift in the emission peak with varying the excitation wavelength) (Fig. 3B) that occurs due to the presence of free zigzag sites, electronic conjugate structures, emissive traps and detects.[97,117,118] The conversion between the lowest unoccupied molecular orbital (LUMO) and the highest occupied molecular orbital (HOMO) can be shown as the PL spectrum. It has been reported that the size of the graphene fragments is dependent on the LUMO–HOMO gap.[6,119,120] Besides, owing to the variable HOMO/LUMO levels with respect to the variation in sizes, GQDs exhibit different excitation and emission spectra. It has also been mentioned that, along with the size, the pH of the GQD colloidal solution also influences the optical properties. In general, GQDs exhibit strong fluorescence at alkaline pH, whereas they show significant fluorescence quenching at acidic pH. These fluorescence changes might occur due to deprotonation and protonation of free zigzag sites present in the GQD structure.[18] By contrast, Shen and co-workers reported that polyethylene glycol (PEG)-passivated GQDs provide a maximum PL intensity at pH 7, which decreases marginally under both acidic and alkaline conditions.[121] The emission quantum energy within GQDs can be confined due to surface passivation and hence provide a higher PL intensity. The thickness of the graphene sheets in the GQDs structure has also been reported for varying the

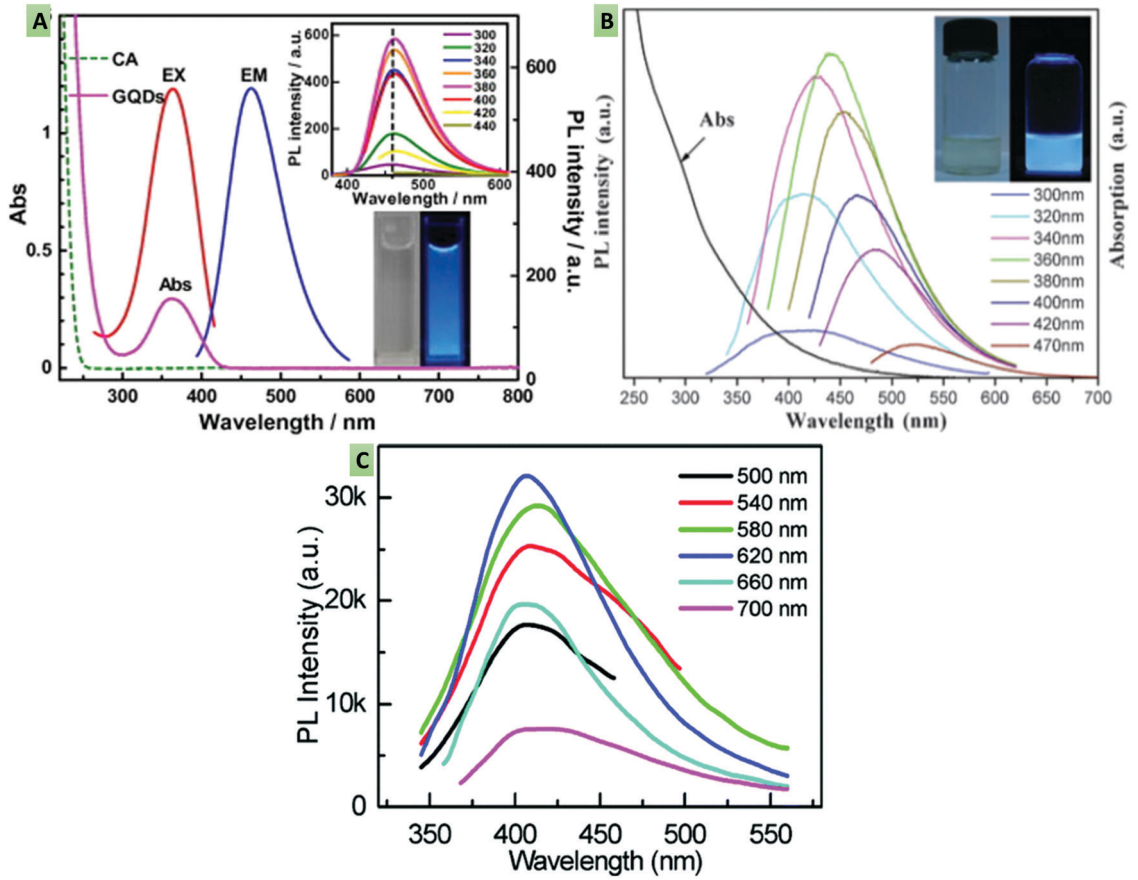

Fig. 3 (A) Excitation-independent emission spectra of blue photoluminescent GQDs under different excitations (300–440 nm), indicating no shift in the emission peak with varying the excitation wavelength (reproduced with permission from ref. 89, copyright 2012 Elsevier B.V.). (B) Excitation-dependent emission spectra wherein there is a shift in the emission peak with varying the excitation wavelength (reproduced with permission from ref. 121, Royal Society of Chemistry). (C) Upconverted emission spectra at different excitation wavelengths (reproduced with permission from ref. 123, copyright 2012 American Chemical Society).

optical properties.[122] It has been observed that the fluorescence intensity is directly proportional to the thickness of the GQDs. In multilayered GQDs, the fluorescent intensity of the topmost layer may be quenched by the untreated lower layers.[122] Another important aspect of the optical properties of GQDs is upconversion luminescence (Fig. 3C).[123] However, the upconversion luminescence phenomenon of GQDs has not yet been explored systematically. Upon excitation with a 900 nm laser, the emission spectrum of GQDs exhibits upconverted green fluorescence. In addition, the emissive peak shifted from 390 to 468 nm when the excitation wavelength was altered from 600 to 800 nm. Furthermore, to approve and clarify these experimental elucidations, a structural model of the GQDs with different energy levels was recommended to investigate the upconversion PL properties. It was explained that electrons in the GQDs were excited to the HOMO level by the laser, and when they revert back to LUMO they emit upconverted PL.[121] Similar to GQDs, CDs have also been found to be highly photoluminescent when excited with an ion laser (458 nm) or *via* two-photon excitation with a femtosecond pulsed laser in the near-infrared region (800 nm). These CDs were used for *in vitro* cell imaging by internalizing them in cancerous cells.[117] Similarly, upconverted PL was observed by Li *et al.*, which was perhaps due to the increased multiphoton activity, as mentioned above.[124]

3.2 Electrochemical properties

Mimicking metallic nanomaterials, graphene has been reported as a zero bandgap material. However, this zero bandgap restricts graphene from emitting light and generating an electron–hole pair upon excitation. If we cut graphene into nanometer sized materials, say GQDs, they can have a non-zero variable bandgap depending upon their size, thereby can emit light upon excitation.[125] Moreover, one of the favorable features of graphene is its lateral conduction in 2D sheets. This property helps in designing electrochemical biosensors for various biomedical applications. However, the difficulty lies in creating electrodes from a single sheet of graphene. By contrast, chemically modified multilayered graphene has numerous defects owing to the introduction of oxygen-containing groups that decrease its lateral conductivity.[14] GQDs, as a derivative of graphene, also possess edge defects, surface-active sites, and a larger surface area. Besides the optical properties, electrochemical properties such as a high current density, fast electron transferability, and good conductivity are widely possessed by GQDs due

to the quantum-confinement and edge effect.[126] Hence, GQDs have been reported to be good transducer material for the development of various electrochemical biosensors with improved signal-to-noise ratio and heterogeneous electron transfer rate.[127,128] Additionally, GQDs are highly dispersible in an aqueous medium owing to the presence of surface functionalities. Furthermore, GQDs can be easily immobilized with biological, inorganic, and organic moieties, essential for the development of numerous electrochemical-sensing platforms.[117]

4. Property regulation of GQDs

Over the past decade, GQDs have received enormous attention from the scientific community owing to their unique optical, biological, electrochemical, and physical characteristics. Further, due to their ease of modification or regulation of these characteristics depending on the specific application, GQDs have emerged as an exciting and indispensable material. In this section, strategies, namely heteroatom doping and surface functionalization, used to regulate the properties of GQDs will be discussed.

4.1 Heteroatom doping

The characteristic features of the GQDs, as we have seen, are primarily due to the physical defects of the graphene sheets. These defects bring about changes in the structural, chemical, and physical properties of graphene nanosheets. These defects are classified into structural, topological, and high-strain folding defects, which mainly occur due to high-temperature annealing, non-sp^2 carbon moieties, and heteroatom doping.[18] The doping-induced effects arise due to the substitution of heteroatoms into the graphene sheets.[129] Depending on the dopants and doping conformations, heteroatom doping facilitates GQDs in providing unique structural and optical properties. A worthwhile method for amending the characteristics of GQDs along with several other nanomaterials is doping them with heteroatoms. The doping process involves the substitution of some C atoms in the GQD matrix with different elements like Si, Se, Cl, S, N, B, P, and F, although it is not limited to these only.[18] The doping crucially enhances the QY, PL intensity, catalytic features, and electrical conductance of GQDs.[95,130–132] In addition, doping has been reported to be advantageous in tailoring the energy bandgap and surface properties of GQDs.[18] There are several methodologies for the incorporation of heteroatoms, which may either be during synthesis (an *in situ* process) or after synthesis (an *ex situ* process). Out of several heteroatoms, N is the most frequently utilized element in GQDs heteroatom doping. This might be ascribed to the greater electronegativity (3.04) of N in comparison with C (2.55), along with the size compatibility (referred to as lesser strain in the lattice) of GQDs.[133] N-GQDs can be synthesized through several processes such as electrochemical, solvothermal/hydrothermal, pyrolysis, microwave methods, *etc.* For example, Kalkal *et al.* described the *in situ* hydrothermal preparation of N-GQDs using CA and DETA as the source of carbon and N dopant, respectively (Fig. 4A). Doping with N enhanced the QY of bare GQDs from 14.57% to 78.83%.[27] Similarly, Hou *et al.* synthesized multilayered N-GQDs that showed intense green fluorescence *via* a microwave-assisted hydrothermal procedure utilizing glucose and urea as the precursors.[134] Li *et al.* reported the preparation of oxygen-rich and electrocatalytically active blue fluorescent N-GQDs *via* an electrochemical method. Compared with their un-doped

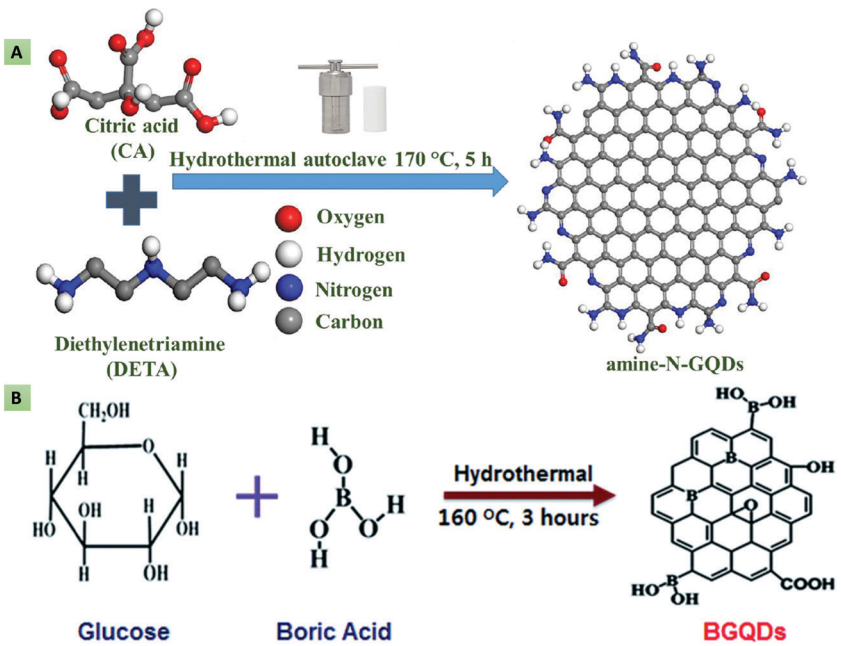

Fig. 4 (A) Nitrogen doping of GQDs using CA and DETA as the C source and N dopant, respectively (reproduced with permission from ref. 27, copyright 2020 American Chemical Society). (B) B-doped GQDs obtained using glucose and H_3BO_3 as the starting materials (reproduced from ref. 130 with permission from Royal Society of Chemistry).

counterparts, the obtained N-GQDs offered an enhanced electrocatalytic activity that was found comparable to the commercially available Pt/C catalyst.[135] Qu *et al.* described the synthesis of a series of N-GQDs *via* hydrothermal method using CA as the carbon source and urea, ethylene diamine (EDA), ethanolamine (EA), diethylene amine (DEA), and hexamethylenetetraamine (HMTA) as the N dopants. It was observed that N-doping considerably increased the QY compared with bare GQDs. Among the different amines, primary diamine (EDA) provided the highest QY of 94%.[136] Recently, Kaur and co-workers reviewed N-doped graphene and GQDs for their utilization in photocatalysts, solar cells, fuel cells, sensors, batteries, and supercapacitors.[137] More recently, Shah *et al.* demonstrated the preparation of green and blue fluorescent N-GQDs employing the oxidative cutting top-down method. Herein, H_2O_2, graphite, methyl-2-pyrrolidone, and ammonium persulfate were used as the oxidizing agent, precursor, solvent, and nitrogen source, respectively. The resultant N-GQDs exhibited good biocompatibility, low toxicity, and superior PL properties.[138] Similarly, Alqarni *et al.* synthesized yellow fluorescent N-GQDs by thermally driven oxidation, wherein H_2O_2, GO, and EDA were used as an oxidizing agent, C source, and N dopant, respectively. The obtained N-GQDs were utilized for dopamine (DA) detection after functionalization with β-cyclodextrin.[139] Tam and colleagues synthesized B-doped GQDs (Fig. 4B) *via* the hydrothermal treatment of boric acid (H_3BO_3) and glucose. It was observed that the existence of B atoms generated multiple active sites, thereby improving the electrocatalytic activity.[130] Budak *et al.* demonstrated the preparation of dual-emissive B- and N-doped GQDs employing the bottom-up hydrothermal method, using 3-aminophenylboronic acid as the boron, nitrogen, and carbon source. Later, H_3BO_3 was added to increase the B-doping content that regulated the dual-emissive property of the B,N-GQDs.[140] In another study, Gu *et al.* reported the synthesis of B and N co-doped GQDs *via* the solvothermal method for electrocatalytic glucose oxidation. The resultant GQDs showed a considerably higher catalytic activity compared with N-GQDs.[141] Zhang *et al.* produced B-GQDs *via* a hydrothermal method by cutting B-doped graphene. It has been mentioned that the B doping enhances the optical properties by introducing a new kind of surface state. Following the principle of aggregation-induced PL enhancement, B-GQDs were utilized in selective glucose detection.[142] Apart from B and N, additional doping agents such as F, P, S, *etc.*, have been reported to modulate the GQD properties. In line with this, Li and co-workers reported the preparation of S-doped GQDs (S-GQDs) *via* the electrolysis of graphite in sodium *p*-toluenesulfonate solution. The S-GQDs were found to possess improved chemical and electronic properties.[143] Similarly, Kadian *et al.* synthesized S-GQDs by the direct pyrolysis of CA and MPA, and discussed the effect of S doping on the QY and fluorescence of the GQDs through both theoretical and experimental investigations. The authors demonstrated that the S doping considerably improved the fluorescence intensity and quantum yield.[20]

In another study, Atar *et al.* utilized the S-GQD based nanocomposite in the detection of interleukin 6 (IL-6) using a quartz crystal microbalance (QCM) immunoassay.[144] Jlassi and their team synthesized N,S-GQDs using graphite waste as the starting material. The obtained GQDs after treatment with NH_3 were spin-coated on an indium tin oxide (ITO)-coated glass substrate for their usage in humidity sensing application.[145] Sangam and co-workers utilized the second-generation (2G) bio-waste (sugarcane molasses) in a hydrothermal method toward the production of highly crystalline, catalyst-free, economical, and large-scale S-GQDs. The as-synthesized GQDs exhibited excellent biocompatibility, and a high QY along with a longer decay time, and were utilized in bioimaging applications.[146] Nair *et al.* demonstrated the rapid production (within 5 min) of S-GQDs *via* a microwave-based sonochemical approach, using GO, $KMnO_4$ and H_2SO_4 as the precursor, oxidizing agent, and the S dopant, respectively (Fig. 5A). The resultant S-GQDs were employed for the highly sensitive detection of carbamate pesticides.[147]

Mondal *et al.* described the hydrothermal synthesis of N and S co-doped GQDs using GO and thiourea as the starting materials. The N,S-GQDs showed an enhanced fluorescence-quenching effect in contrast to monoatomic-doped GQDs for trinitrophenol (TNP) detection.[148] In another study, Li *et al.* reported the electrochemical synthesis of P-doped GQDs (Fig. 5B) utilizing a carbon electrode and sodium phytate as the C source and P dopant, respectively.[68] These reports showed that the type of dopant, particularly its size and charge, influences the properties of the GQDs, and further these dopants have the ability to tailor the energy bandgap as well as the surface properties of GQDs, thereby augmenting the QY and photoelectric attributes of GQDs.[143] Wang *et al.* demonstrated the preparation of S and P co-doped GQDs *via* a one-pot, non-toxic, and rapid hydrothermal approach using CA, anhydrous sodium sulfate and sodium phytate as the C, S, and P sources, respectively. The as-prepared GQDs revealed a high tolerance of ionic strength, pH sensitivity (in the range of 8.0–13.0), excitation-dependent behavior, and an improved QY compared with individual S- or P-doped GQDs.[149] Instead, Liu and co-workers described the synthesis of P,N-GQDs based on EDA end-capped polyethylenimine (PEI) and hydroxymethyl phosphonium chloride as the precursors. The obtained GQDs showed remarkable biocompatibility, concentration- and excitation-dependent behavior, a high QY and good water dispersibility.

4.2 Surface functionalization

The other strategy that influences the optical, physical, and electrochemical properties of GQDs is surface- or edge-modification with electron-donating/accepting, hydroxyl (–OH), carboxyl (–COOH) and amine ($–NH_2$) groups and other biomolecules.[150] The surface modification of GQDs can be performed either during their synthesis by introducing raw materials that contain the required functional groups, or after synthesis, *via* attachment of the desired functionalities. Initially, Qian *et al.* demonstrated (Fig. 6A) that the functionalization of GQDs with diamine significantly regulates their optical characteristics and QY due to their unique protonation phenomenon.[151] It has also been observed that primary amine-functionalized GQDs also possess improved optical properties

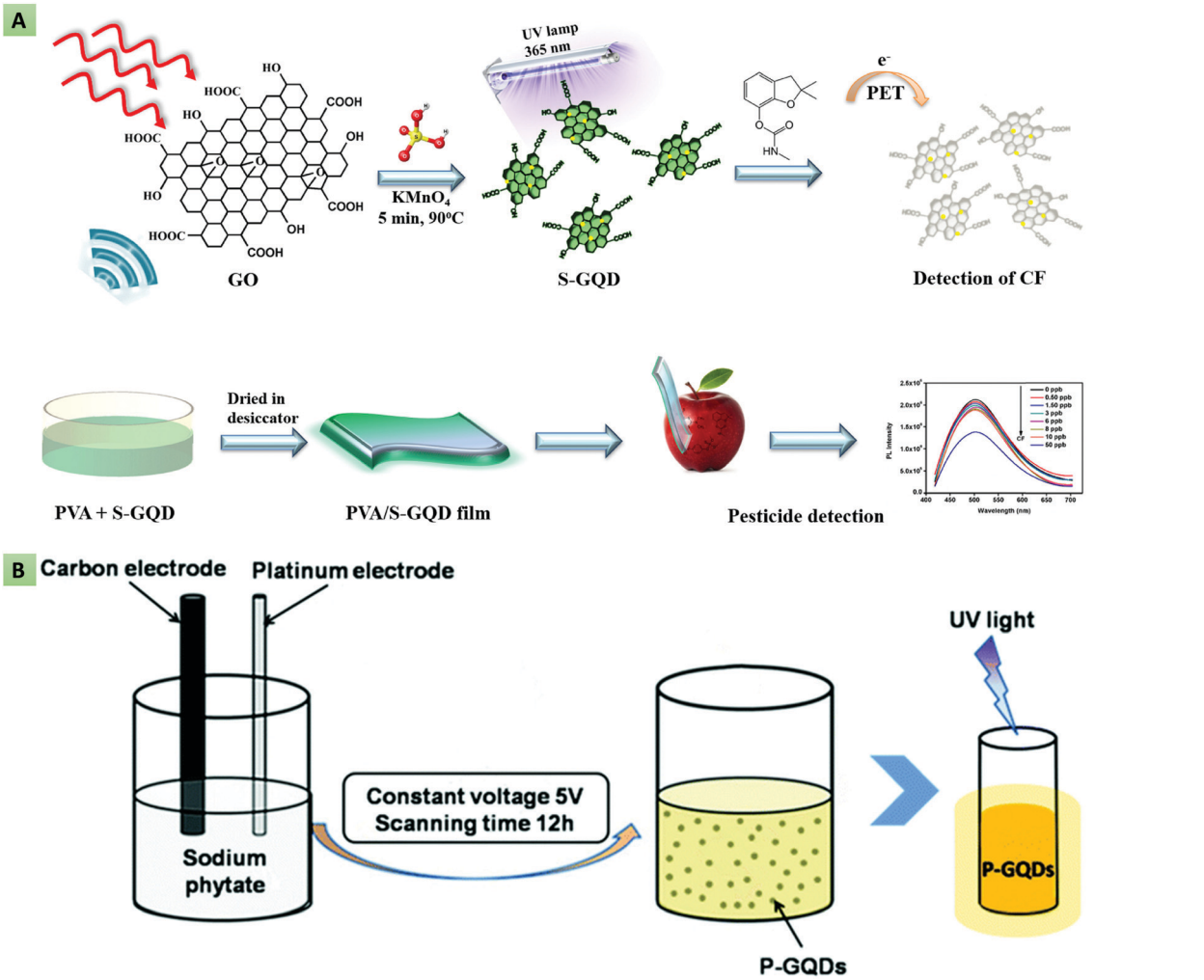

Fig. 5 (A) Synthesis of S-doped GQDs *via* a microwave approach for pesticide detection (reproduced with permission from ref. 147, copyright 2020 Elsevier B.V.). (B) Electrochemical synthesis of P-doped GQDs using a carbon electrode as the C source and sodium phytate as the P dopant (reproduced from ref. 68 with permission from the PCCP owner societies).

compared with bare GQDs. In line with this, Sun *et al.* reported the amine functionalization of GQDs in the presence of NH_3 *via* a hydrothermal route. The amine functionalization converted the yellow-green fluorescent GQDs having low QY (2.5%) to blue fluorescent GQDs having an improved QY (16.4%).[152] Similarly, in order to tailor the optical and electronic properties, Tetsuka and co-workers described the synthesis of amino-GQDs (Fig. 6B) using GO and NH_3 as precursors.[153]

In another study, Wang *et al.* described the preparation of yellow fluorescent amino-GQDs *via* the hydrothermal method by utilizing NH_3 as the N source and asphalt as the precursor material. The amino functionalization enriched n–π* electron transitions, leading to improvement in the PL QY from 4.7% (bare GQDs) to 13.8%.[154] Tam and Choi reported a one-pot, simple, and green hydrothermal method toward the production of bright green fluorescent amino-GQDs without using any toxic chemical reagent, oxidant, or strong acid. Glucose and ammonium were utilized as the C source and *in situ* functionalizing agent, avoiding the need for post-surface passivation or modification. The obtained amino-GQDs indicated a better QY along with an improved quenching ability for the efficient detection of copper (Cu^{2+}) ions.[155]

Moreover, PEI and polyethylene glycol (PEG) have been found to be useful passivating moieties, which, apart from improving the optical properties of GQDs, generate supplementary binding sites for further biomolecule immobilization. In this context, Jin *et al.* reported that GQDs surface-functionalized with PEG-diamine indicate a red shift in their PL emission spectra.[156] This shift can be accredited to the prominent charge transfer between the GQDs and the amino functional groups. Wang and colleagues loaded an anti-cancer drug on the binding sites produced by the PEG functionalization of green-fluorescent GQDs.[157] Similarly, Shen and co-workers described the synthesis of PEG-functionalized GQDs *via* the hydrazine hydrate (N_2H_4) reduction of oxidized PEG-GO. The resultant GQDs revealed upconversion green fluorescence under 980 nm laser irradiation and intense blue fluorescence under 365 nm excitation.[121] Later the same group also reported the hydrothermal synthesis of PEG

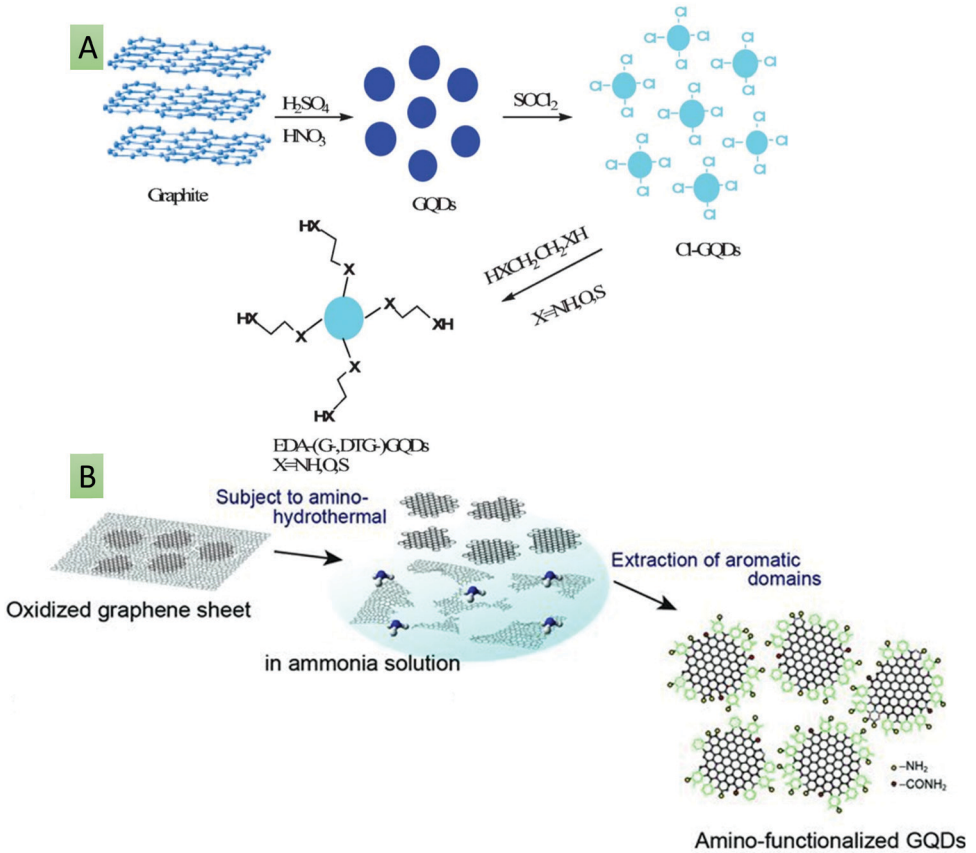

Fig. 6 (A) GQD surface functionalization with dithioglycols, glycols, and diamines for the tuning of optical properties (reproduced from ref. 151 with permission from Royal Society of Chemistry). (B) Synthesis of amino-GQDs using GO and NH_3 as precursors (reproduced with permission from ref. 153, copyright 2012 Wiley-VCH).

surface-passivated GQDs utilizing GO and PEG as the starting materials. The as-synthesized GQDs exhibited upconversion blue fluorescence under 808 nm laser irradiation. Besides, the PEG-GQDs indicated a better photocurrent generation ability and double QY compared with the bare GQDs.[118] Lou and their team described the hydrothermal treatment of cane molasses to obtain PEG-GQDs for metal-ion detection. The PEG functionalization provided intense blue fluorescence along with an improved QY in contrast to bare GQDs.[158] Wang *et al.* demonstrated the hydrothermal preparation of GQDs using coffee grounds and N_2H_4 as the starting materials. The as-prepared GQDs were further surface-functionalized with PEI and revealed enriched band-edge PL characteristics. Besides, the prepared PEI-GQDs were utilized for sensing and bioimaging applications owing to their high selectivity and low cytotoxicity.[159] Likewise, Achadu *et al.* synthesized PEI-GQDs for the development of a fluorescent turn-on sensing probe for the detection of biothiols. The surface functionalization of GQDs with PEI bestowed positive charge and surface passivation, enabling the efficient fluorescence quenching with the Au@Ag core–shell nanomaterial. The addition of biothiols restored the quenched fluorescence in view of the strong metal–thiol (Au–S and Ag–S) interactions.[160] Further, Li *et al.* used chlorosulfonic acid to synthesize sulfonated GQDs (S-GQDs) for catalytic applications. It was observed that the as-prepared S-GQDs impart enhanced catalytic activity for the degradation of carbohydrates including fructose, glucose and cellulose.[161] Chowdhury *et al.* described the DA functionalization (Fig. 7) of blue-fluorescent GQDs for determining ferric (Fe^{3+}) ions.[162] Furthermore, the functionalization of GQDs with targeting ligands has been explored for targeted bioimaging and drug-delivery applications.[163,164] In this context, Li and colleagues demonstrated the functionalization of GQDs with folic acid (FA) for cancer-cell imaging.[165] Similarly, Kadian *et al.* reported FA functionalized S-GQDs (FA-SGQDs) for the targeted bioimaging of cancer cells *via* the endocytosis process.[166] Abdullah *et al.* described the hyaluronic acid functionalization of GQDs for targeted cancer-cell imaging and drug-delivery applications.[164] He and co-workers described the synthesis of hemin-functionalized GQDs in fabricating a highly specific and sensitive glucose biosensor. The hemin functionalization enabled H_2O_2 to disturb the passivated GQDs surface, resulting in substantial PL quenching for selective glucose detection.[167]

In another study, Arunragsa *et al.* employed the bottom-up hydrothermal route using pyrene as the starting material for preparing hydroxyl-functionalized GQDs (OH-GQDs). The prepared OH-GQDs were utilized for the rapid, selective, and ultrasensitive detection of NH_3 owing to the presence of –OH groups (Fig. 8).[168] Guo *et al.* described the surface functionalization of GQDs with rhodamine B in developing a selective and sensitive nanosensor for Fe^{3+} ion detection. The resultant GQDs showed better

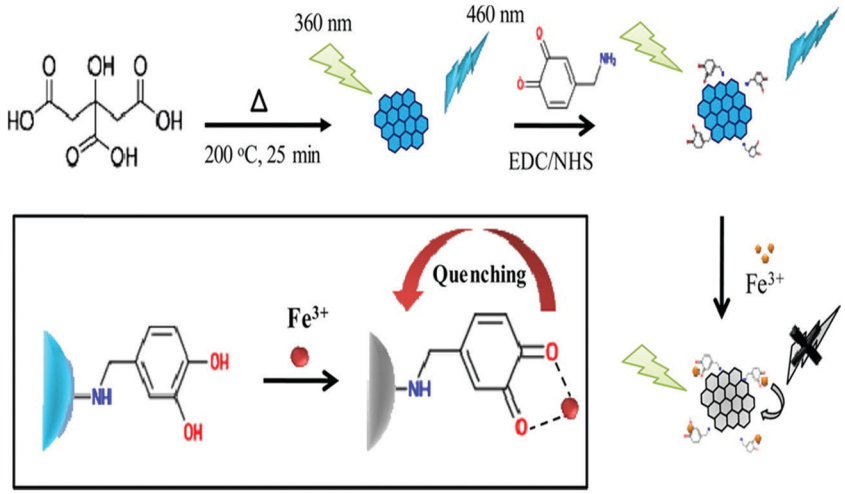

Fig. 7 Surface functionalization of GQDs with DA using EDC/NHS chemistry by activating the –COOH groups of GQDs and coupling with the $-NH_2$ groups of DA (reproduced with permission from ref. 162, copyright 2016 American Chemical Society).

biocompatibility, sensitivity, photostability, and water solubility for efficient Fe^{3+} ion detection with a limit of detection (LOD) of 0.02 μM.[169] Recently, Park *et al.* described the surface functionalization of GQDs with hexadecylamine (HDA), PEG, and polyhedral oligomeric silsesquioxane (POSS) for reducing aggregation-caused PL quenching.[170] Thus, it may be conferred that the properties of GQDs can be regulated by the addition of raw precursors during or after synthesis as per the desired application.

5. Biosensing applications of GQDs

GQDs have been considered as a predominant material in the fabrication of advanced optical and electrochemical biosensors in view of their exciting properties such as an abundance of active sites, remarkable biocompatibility, high current density, fast electron transferability, desired aqueous solubility, good photochemical stability, ease of surface regulation and high QY. GQDs can interact with different biological, inorganic, and organic molecules through electrostatic interactions and π–π conjugation, making them viable for fabricating biosensing platforms.[171] Various biomolecules can be covalently immobilized to GQDs, preventing their aggregation and providing minimum steric hindrance to their active sites. Besides, GQDs can act as either an electron-transfer mediator or an electric wire for enhancing the electron-transfer rate between the electrode surface and the active sites of biomolecules. In the case of optical-biosensing platforms,

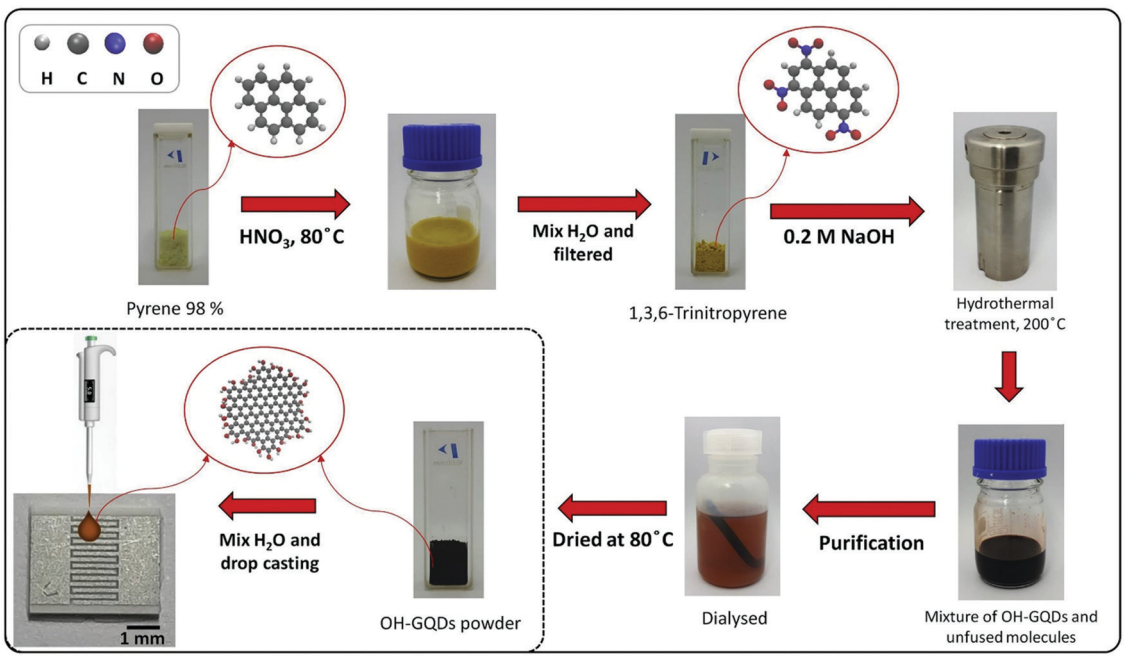

Fig. 8 Preparation of OH-GQDs and their utilization for NH_3 detection (reprinted with permission from ref. 168, copyright 2020 Elsevier B.V.).

GQDs are used as efficient fluorescent donors. The current section will highlight the recent advancements in GQD-based fluorescent, electrochemiluminescent, and electrochemical biosensing platforms.

5.1 Optical biosensors

The interface between biomolecules and GQDs can significantly quench the inherent fluorescence of GQDs. Based on this phenomenon, several chemical sensors, chemosensors and biosensors have been developed to detect small molecules, nucleic acids, bioflavonoids, amino acids, vitamins, heavy metal ions, and biomarkers with enhanced sensitivity and selectivity.[27,84,172] The development of these optical-sensing probes has paved a new pathway for fabricating next-generation point-of-care diagnostic tools to manage several life-threatening diseases and environmental safety. Generally, the optical biosensors include a light-emitting source, a photo-detector for assessing the optical signal, and a bio-receptor.[173] In line with this, Li and co-workers reported the histidine- and pentaethylenehexamine-functionalized GQDs (PEHA–GQD–His) for determining microRNA (miRNA). The PL intensity of the functionalized GQDs was found to be decreased linearly in the dynamic range of 1×10^{-18} to 1×10^{-12} M. The fluorescent biosensor was able to detect the target microRNA-141 in human serum with a LOD of 4.3×10^{-19} M.[174] It has been mentioned that PEHA–GQDs–His provides improved catalytic activity and strong fluorescence emission. Kermani *et al.* designed a DNA-functionalized GQD-based optical-biosensing assay for observing the activity of M.SssI methyltransferase (M.SssI MTase). The mentioned assay exhibited interesting biosensing characteristics with a LOD of 0.7 U mL^{-1} towards M.SssI determination.[175] Ahmed *et al.* designed a GQD-based aptasensor for the label-free and rapid detection of tetracycline in food samples with a LOD of 18 ng mL^{-1}.[176] In this study, GQDs were utilized as the energy donor, and PdNPs were utilized as the energy acceptor. Ruiyi and their team fabricated a sensitive nanoprobe for carbendazim quantification based on histidine and serine co-functionalized GQDs (Ser–GQDs–His). The fabricated probe exhibited a higher sensitivity and selectivity with a LOD of 6.1×10^{-17} M over the linear correlation from 1.0×10^{-16} to 1.0×10^{-9} M.[177] Arunragsa *et al.* employed OH-GQDs for the rapid, selective, and ultrasensitive detection of NH_3 in the dynamic range of 10–500 ppm.[168] He and co-workers reported a glucose oxidase (GOx)- and hemin-functionalized GQDs-based highly specific and sensitive glucose biosensor. The hemin functionalization of the GQDs enabled H_2O_2 to disturb the functionalized GQDs surface, resulting in substantial PL quenching for the selective detection of glucose with a LOD of 0.1 μM.[167] Farahani and co-workers developed a fluorescent nanosensor based on H_3BO_3-functionalized S,N co-doped GQDs for the efficient detection of glucose with a LOD of 5.5 μM.[178] The nanosensor mechanism relies on recovery of the fluorescence intensity after the addition of the target analyte. The addition of glucose restricts non-radiative intramolecular motions due to binding of the H_3BO_3 groups of the GQDs with the *cis*-diol groups of glucose, resulting in fluorescence recovery. Sun *et al.* demonstrated (Fig. 9A) a fluorescent biosensor using N-GQDs and chromium picolinate (CrPic) towards the detection of cholesterol with a LOD of 0.4 mM over the dynamic range of 0–520 mM.[179] The N-GQDs offered convenient surface grafting, strong resistance to photobleaching, and the superior biocompatibility required for the fabrication of an efficient fluorescent biosensor. Ryu *et al.* fabricated a highly selective fluorescent biosensor using europium (Eu)–macromolecule-functionalized GQDs for detecting *Bacillus anthracis* spores. The Eu-GQD-based sensor validated the quantity of *B. anthracis* with a LOD of 10 pM and a detection time of 8 s. This rapid detection was ascribed to the larger surface-area-to-volume ratio of the GQDs, providing efficient contact with the target analyte.[180]

Based on the principle of a fluorescence turn-on assay, Liu *et al.* reported a GQD-based fluorescent probe for the detection of ascorbic acid (AA) in human serum samples. It was observed that the fluorescence intensity varied linearly, with the concentration of H_2O_2 ranging from 3.33 to 500 μM.[182] Similarly, Li *et al.* reported (Fig. 9B) a GQD and cytochrome *c* (Cyt *c*)-based turn-on biosensor for the detection of trypsin, showing a LOD of 33 ng mL^{-1} and a detection range of 1–400 μM.[181] The addition of Cyt *c* provides the self-assembled aggregation of GQDs, leading to fluorescence quenching, whereas trypsin addition prevents aggregation of the GQDs and hence results in gradual recovery of the PL intensity. Another study by Na *et al.* reported a novel approach for detecting AA along with the alkaline phosphatase (ALP) enzyme, based on the similar principle of a fluorescence "turn off–on" assay. In this assay, MnO_2 nanosheets quenched the fluorescence of sulfanilic acid-functionalized GQDs, and the addition of ALP/AA triggered disintegration of the MnO_2 nanosheets and resulted in the linear recovery of quenched fluorescence of GQDs.[183] Kongsanan and their team developed a fluorescent switch (turn-on–off) sensing platform based on mercuric cation (Hg^{2+})-decorated GQDs toward the selective and simultaneous detection of ferricyanide $[Fe(CN)_6]^{3-}$ and cyanide (CN^-). The Hg^{2+} decoration quenched the inherent blue fluoresce of the GQDs, termed as the baseline state. The addition of CN^- enables restoration of the quenched GQD fluorescence (turn-on), whereas the addition of $[Fe(CN)_6]^{3-}$ again quenched the fluorescence to the turn-off state. The as-fabricated sensing platform exhibited LOD values of 9.48 and 3.10 μM with the linear detection ranges of 10.0–50.0 μM and 5.0–15.0 μM for $[Fe(CN)_6]^{3-}$ and cyanide (CN^-), respectively.[184] Wang *et al.* fabricated a glucose-biosensing platform based on the fluorescence quenching and restoration of GOx enzyme-coupled GQDs and exhibited a linear correlation between the glucose concentration and the PL intensity over the dynamic range of 0.2–10 μmol L^{-1}.[185] Further, Qu *et al.* designed GSH-functionalized GQDs and a Fe^{3+} ion-based fluorescent "off–on" sensor toward the sensitive detection of phytic acid and H_2O_2.[186] The as-prepared sensing probe exhibited good linearity between the concentration of phytic acid/H_2O_2 and the GQDs–GSH PL intensity ranging from 0.05 to 3 μmol L^{-1} and 0.5 to 10 μmol L^{-1}, respectively. The interaction between the carboxyl surface groups of GQDs–GSH and Fe^{3+} ions results in the formation of the Fe^{3+}/GQDs@GSH complex, wherein electrons

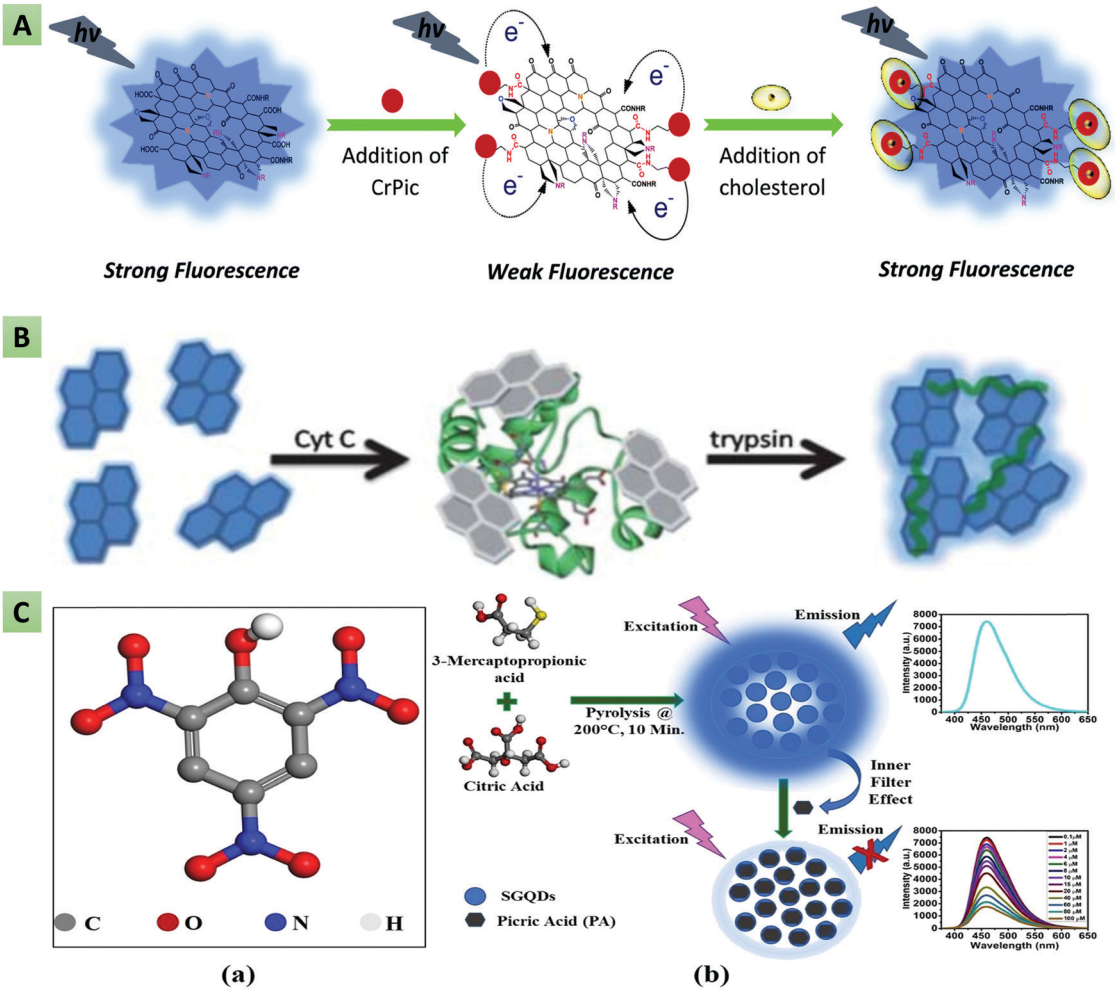

Fig. 9 (A) N-GQD and chromium picolinate-based fluorescent nanoprobe for cholesterol detection (reproduced from ref. 179 with permission from Royal Society of Chemistry). (B) Self-assembled GQDs for trypsin detection (reproduced from ref. 181 with permission from Royal Society of Chemistry). (C) S-GQDs for picric acid detection based on the inner filter effect (reprinted with permission from ref. 84, copyright 2020 Wiley and Sons).

are transferred from GQDs@GSH to the Fe^{3+} ions, and the fluorescence is quenched *via* the photo-induced electron-transfer (PET) process. In another study, Guo and co-workers reported the rhodamine B surface-functionalized GQD-based selective and sensitive nanosensor for Fe^{3+} ion detection in cancer stem cells. The resultant GQDs showed better biocompatibility, sensitivity, photostability, and water solubility for the efficient detection of Fe^{3+} ions with a LOD of 0.02 μM.[169] Similarly, Lou *et al.* described the quantification and detection of Fe^{3+} ions using PEG-GQDs as a selective nanoprobe with a LOD of 5.77 μM.[158] Recently, Wu *et al.* reported a sensitive fluorescent sensing probe for Fe^{3+} ion detection in HeLa cells and water samples with a LOD of 1.43 nM in the dynamic range of 0.02–12 μM.[187]

Sahub *et al.* used GQDs for the development of an optical pesticide sensor through the enzymatic reaction of choline oxidase (CHOx) and acetylcholinesterase (AchE) for the sensitive detection of organophosphate pesticide in water and food samples.[188] Mondal and their team prepared a N,S-GQD-based fluorescent sensing probe for TNP detection with a LOD of 19.05 ppb.[148] Next, Zhang *et al.* reported the efficient detection of glucose using B-doped GQDs. The presence of boronic groups on the edges of the B-GQDs enabled interaction with the *cis*-diol units of glucose, forming B-GQDs–glucose aggregates that lead to restoration of the GQDs PL intensity.[142] Ananthanarayanan *et al.* used electrochemically exfoliated GQDs toward the selective quantification of Fe^{3+} ions (LOD ≈ 7.22 μM).[189] Similarly, Patra and co-workers prepared a nanohybrid of CdS-doped 2D graphene sheets and GQDs with enhanced optical properties to effectively detect nimesulide in urine, plasma, and blood serum samples with a LOD of 6.65 ng L^{-1}.[190] Kadian *et al.* demonstrated the selective and specific fluorescent sensing probe based on the inner filter effect (IFE) for picric acid (PA) detection (Fig. 9C). The inherent fluorescence of SGQDs decreased gradually with the addition of PA over the detection range of 0.1–100 μM.[84] SGQDs were advantageous in minimizing the effect of autofluorescence during PA detection and revealed excitation-independent emission spectra. Amjadi *et al.* utilized the strong chemiluminescence (CL) properties of molecularly imprinted polymer-capped N-GQDs (MIP@N-GQDs) for the

determination of doxorubicin. The doping of GQDs with N atoms provided excellent CL properties.[191] Similarly, Chen and colleagues developed a Cu^{2+} ion-catalyzed N-GQD-based CL sensing system toward the selective determination of AA with a LOD of 0.5 μM.[192] Hassanzadeh *et al.* designed another non-enzymatic CL sensing probe using a mixture of GQDs and MoS_2 QDs to monitor the cholesterol concentration in human serum with a LOD of 35 nmol L^{-1}.[193] The analytical figure of merit has been ascribed to the synergetic effect of electronic interactions between the GQDs and MoS_2 QDs. Further, Al-Ogaidi developed a chemiluminescence resonance energy transfer (CRET) based immunosensor for rapid and selective monitoring of ovarian cancer biomarker by using GQDs as an energy acceptor. The as-prepared sensing probe revealed good linearity in the range from 0.1 U mL^{-1} to 600 U mL^{-1} with a LOD of 0.05 U mL^{-1}.[194]

Similar to CRET, nanosurface energy transfer (NSET) and fluorescent resonance energy transfer (FRET) are other important optical phenomena wherein the energy of the fluorophore (donor) is transferred non-radiatively to nearby acceptor species. These are distance-dependent phenomena that rely on the efficient overlap between the emission spectra of the donor and the absorption spectra of acceptor species. Energy-transfer-based biosensors have been widely used to observe nanoscale information and biomolecular interactions.[27] For instance, Qian and colleagues described a reproducible FRET-based sensing system using GQDs and CNTs as the energy donor–acceptor pair for the ultrasensitive quantification of DNA with a LOD of 0.4 nM.[195] The GQDs provided a higher FRET efficiency, strong fluorescence, and good biocompatibility, and hence worked as the excellent fluorophore in the fluorescent biosensor fabrication. Similarly, Na *et al.* designed another ultrasensitive FRET pair between Nile red (NR) and GQDs through electrostatic interaction *via* the lecithin/β-cyclodextrin (lecithin/β-CD) complex for determining the concentration of acid phosphatase with the LOD of 28 μU mL^{-1}.[196] In this biosensing system, GQDs worked as the fluorescent donor and the support material for attaching the lecithin/β-CD complex through hydrophobic and electrostatic interactions. Next, Yan *et al.* reported a GQD (donor) and AuNP (acceptor)-based turn-on FRET sensor to determine the concentration of glutathione reductase (GR) in human serum samples.[197] Interaction of the AuNP and GQD colloidal solution initiates the aggregation, leading to GQD fluorescence quenching. The quenched fluorescence was found to recover gradually after the selective addition of GR. Kalkal *et al.* demonstrated (Fig. 10) the fabrication of an NSET biosensor based on gold nanoparticles (AuNPs) and amine-functionalized N-doped GQDs (amine-N-GQDs) for the ultrasensitive determination of neuron-specific enolase (NSE). The as-fabricated biosensor exhibited remarkable biosensing characteristics, including a low LOD (0.09 pg mL^{-1}), a wide linear detection range (0.1 pg mL^{-1} to 1000 ng mL^{-1}), and a fast response time (16 min).[27] The better sensing characteristics were attributed to *in situ* $-NH_2$ functionalization and N doping of GQDs providing stable and strong PL, a long fluorescence lifetime, and improved QY. Further, Sun and colleagues developed an ultrasensitive nanoprobe for miRNA-34a detection *via* an ''off–on'' FRET system between GQDs and gold nanoflowers (AuNFs).[198] Similarly, Shi *et al.* reported a FRET nano biosensor based on AuNPs and GQDs toward determining the *mec*A gene sequence of foodborne bacteria. Herein, GQDs were utilized to immobilize the capture probe and fluorescent donor in the FRET system.[199] Poon and co-workers designed a coumarin derivative (CMR2) and GQD-based FRET system for the sensitive detection of trypsin in urine samples.[200] Similarly, Laurenti *et al.* fabricated a fluorescent biosensing platform using single-stranded DNA (ssDNA)-functionalized upconversion nanoparticles and

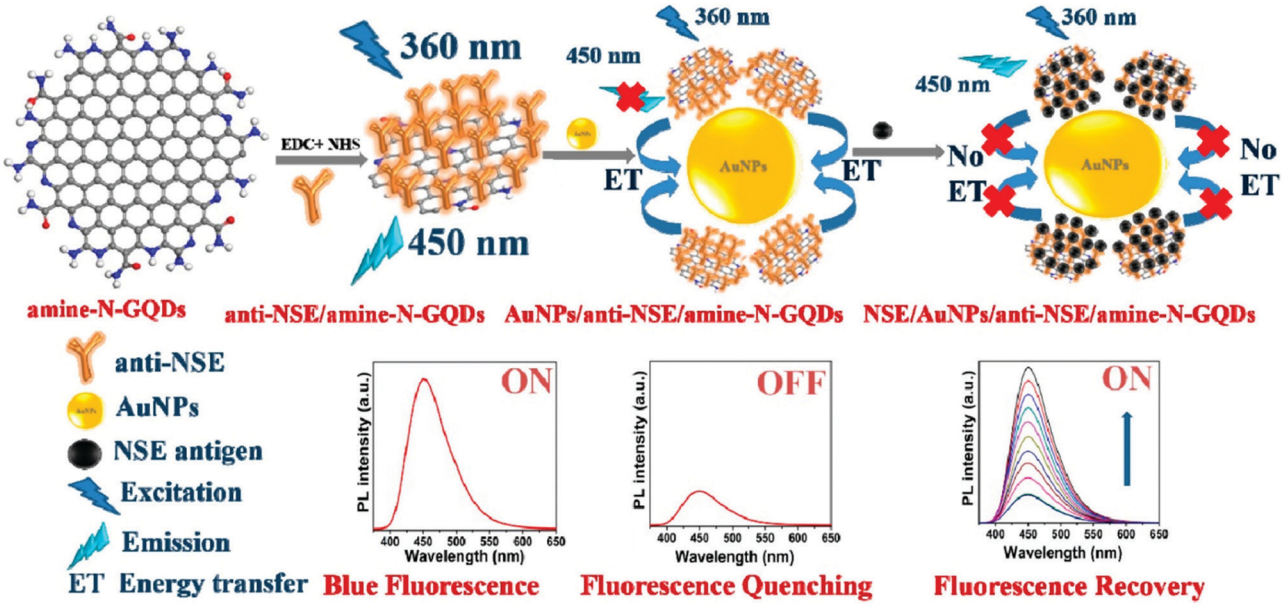

Fig. 10 Amine-N-GQD- and AuNP-based fluorescent turn-on biosensor for neuron-specific enolase (NSE) detection (reproduced with permission from ref. 27, copyright 2020 American Chemical Society).

GQDs for the detection of the miRNA sequence.[201] It was found that the upconversion fluorescence increases in the absence of complementary miRNA. At the same time, the fluorescence intensity decreased linearly upon hybridization with complementary miRNA sequences. The as-proposed sensing probe achieved a LOD of 10 fM. Wang *et al.* demonstrated a fluorescent turn-on sensing probe for GSH detection using manganese dioxide (MnO_2) and GQDs. The blue fluorescence of the GQDs was remarkably quenched by the MnO_2 nanoparticles following FRET and IFE mechanisms. Further, the addition of GSH linearly recovered the GQD quenched fluorescence in the dynamic range of 0.07–70 μM.[202] Recently, Kamal *et al.* (Fig. 11) reported a fluorescent immunosensor for *Salmonella typhi* (*S. typhi*) detection utilizing iron porphyrin bio-mimicked GQDs (Fe–N-GQDs) and GO as the FRET donor–acceptor pair. The reported immunosensor exhibited efficient sensing characteristics for the detection of *S.* Typhi with a LOD of 1 pg mL^{-1} and a linear correlation from 1 pg mL^{-1} to 1 μg mL^{-1}.[203] In another study, Xue and co-workers described the detection of melamine in milk samples utilizing GQDs and protoporphyrin IX (PpIX) as the FRET pair. The binding of PpIX to the GQDs triggered the FRET process, resulting in fluorescence quenching of the GQDs. However, the addition of melamine enabled recovery of the quenched fluorescence by inhibiting the FRET process. This FRET-based sensing platform revealed accurate and quick melamine detection with a LOD of 6×10^{-9} mol L^{-1} over a dynamic range from 1.0×10^{-8} to 2.0×10^{-6} mol L^{-1}.[204] Table 2 summarizes different GQD-based fluorescent biosensors along with their sensing characteristics.

5.2 Electrochemiluminescence based optical biosensors

Electrochemiluminescence (ECL) is a type of luminescence generated during electrochemical reactions. A basic ECL sensor includes reference, counter, and working electrodes as the necessary components. In a recent study, Lou and co-workers[207] demonstrated the role of the GQDs in the development of an ECL-based sensing probe to quantify DNA through site-specific endonuclease (*Bam*HI) cleavage of the duplex. Next, Tian and colleagues prepared GQDs through the photochemical and

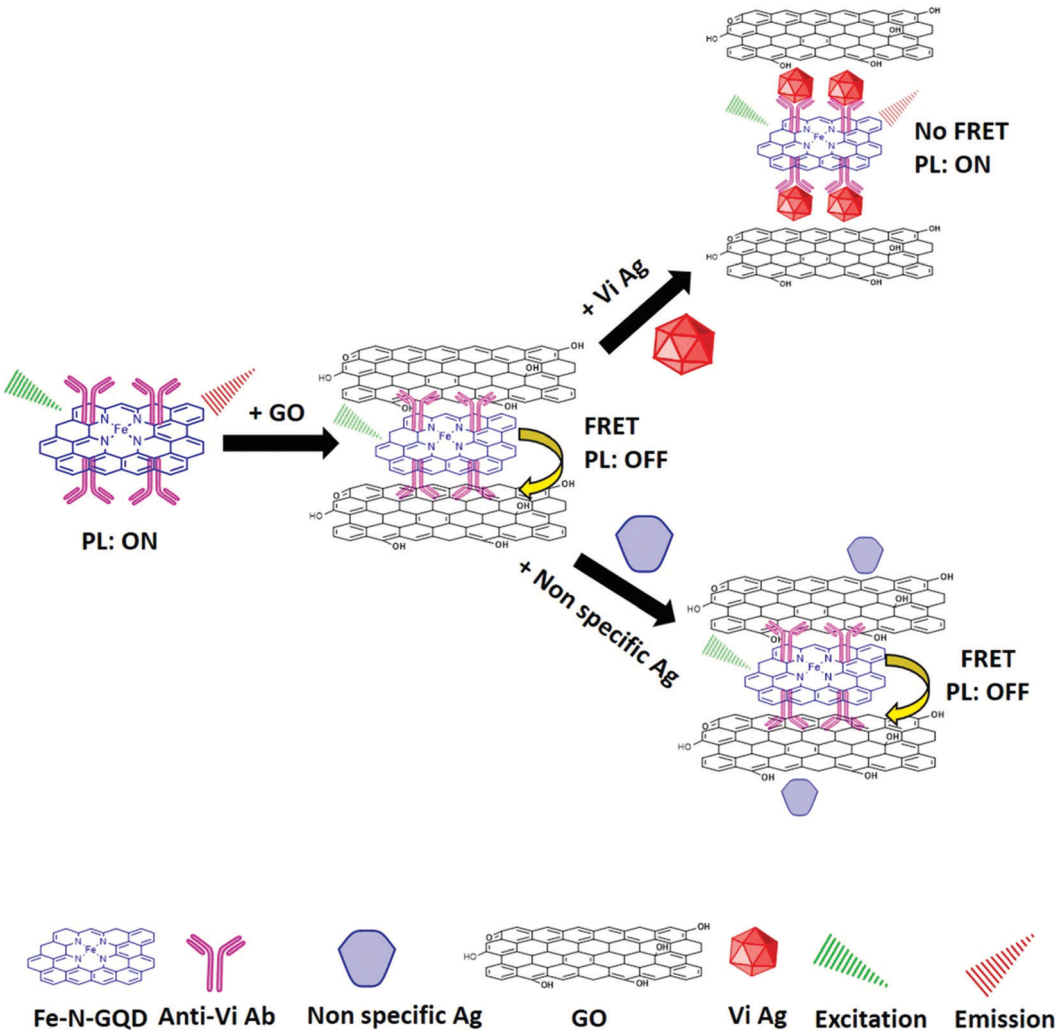

Fig. 11 Schematic representation of the fluorescent immunosensor for *Salmonella* Typhi (*S. typhi*) detection utilizing iron porphyrin bio-mimicked GQDs (Fe–N-GQDs) and GO as the FRET donor–acceptor pair (reproduced with permission from ref. 203, copyright 2021 Elsevier B.V.).

Table 2 Summary of different GQDs based fluorescent biosensors along with sensing characteristics

Sensing platform	Analyte detected	LOD	Time (min)	Detection range	Ref.
PEHA–GQD–His	microRNA	4.3×10^{-19} M	—	1×10^{-18} to 1×10^{-12} M	174
ds DNA/GQDs	M.SssI Mtase	0.7 U mL^{-1}	40	2–30 U mL^{-1}	175
PdNPs/aptamer/GQDs	Tetracycline	18 ng mL^{-1}	5	40–90 ng mL^{-1}	176
H_3BO_3-S,N-GQDs	Glucose	5.5 μM		5.5–66 mM	178
N-GQDs/CrPic	Cholesterol	0.4 μM	5	0–520 μM	179
Eu-GQDs	*Bacillus anthracis*	10 pM	0.13	0–5 nM	180
HRP-GQDs	AA	0.32 μM	45	1.11–300 μM	182
Cyt c-GQDs	Trypsin	33 ng mL^{-1}	1440	0–400 μM	181
MnO_2/GQDs	AA	0.045 U L-	10	0.13–10 U L^{-1}	183
	Alkaline phosphatase				
GQDs-GOx-HRP	Glucose	0.08 μmol L^{-1}	80	0.2–10 μmol L^{-1}	205
Ser–GQDs–His	Carbendazim	6.1×10^{-17} M	—	1.0×10^{-16} to 1.0×10^{-9} M	177
GQDs-GOx-hemin	Glucose	0.1 μM	10	9–300 μM	167
GQDs@GSH	Phytic acid	14 nmol L^{-1}	6	0.05–3 μmol L^{-1}	186
	H_2O_2	0.134 μmol L^{-1}	40	0.5–10 μmol L^{-1}	
GQDs/AchE/CHOx	Methyl-paraoxon	0.342 μM	30	0.40–4.05 μM	188
N,S-GQDs	TNP	19.05 ppb	—	100–25 000 nM	148
SGQDs	Picric acid	0.093 μM	—	0.1–100 μM	84
MIP@N-GQDs	Doxorubicin	4.7 μg L^{-1}	5	20–260 μg L^{-1}	191
MoS_2/graphene QDs	Cholesterol	35 nmol L^{-1}	5	0.08–300 μmol L^{-1}	193
GQDs–cAb	CA-125	0.05 U mL^{-1}	—	0.1 U mL^{-1} to 600 U mL^{-1}	194
ssDNA–rGQDs/CNT	DNA	0.4 nM		0–133.0 nM	195
GQDs-NR	Acid phosphatase	28 μU mL^{-1}	90	0–1500 μU mL^{-1}	196
GQDs-AuNPs	GSH	0.005 mU mL^{-1}	15	0.005–0.13 mU mL^{-1}	197
Amine-N-GQDs@AuNPs	Neuron specific enolase	0.09 pg mL^{-1}	16	0.0001–1000 ng mL^{-1}	27
AuNF@GQDs	miRNA-34a	0.1 fM	—	0.4–4 fM	206
GQDs–AuNPs	*mecA*			100 pM to 400 nM	199
GQDs/UCNP@SiO_2	Trypsin	0.7 μg mL-	60	0–23 μg mL^{-1}	200
RBD-GQDs	Fe^{3+}	0.02 μM		0–65 μM	169
GQDs-Hg^{2+}	$[Fe(CN)_6]^{3-}$ and CN^-	9.48, 3.10 μM	—	0.0–50.0 and 5.0–15.0 μM	184
Fe–N-GQDs	*S. typhi*	1 pg mL^{-1}	20	1 pg mL^{-1} to 1 μg mL^{-1}	203
PpIX to GQDs	Melamine	6×10^{-9} mol L^{-1}	20	1.0×10^{-8} to 2.0×10^{-6} mol L^{-1}	204

sonochemical treatment of GO sheets with H_2O_2, and studied their ECL properties for the fabrication of a glucose-sensing platform. It was mentioned that the ECL signal was generated primarily due to the reduction of dissolved oxygen and GQDs. The GQDs provided the cathodic ECL signal that was improved by $K_2S_2O_8$.[208] Chen *et al.* developed a polydopamine surface-imprinted polymer and N-GQDs (PDA-SIP-N-GQDs)-based bio-engineered ECL biosensing platform (Fig. 12) for the quantitative detection of *Escherichia coli* (*E. coli*).[209] The ECL signals were generated *via* the specific antigen–antibody interactions by binding the SIP–*E. coli*-modified electrode to pAb-N-GQDs. In another report, Lu *et al.* synthesized blue-luminescent GQDs with graphitic structure nanocrystals having a QY of 15.5% and demonstrated the ECL resonance energy transfer (ECL-RET) phenomenon of the as-prepared GQDs (donor) and AuNPs (acceptor) for the detection of DNA damage (Fig. 13).[210] The ECL signal of the GQDs was

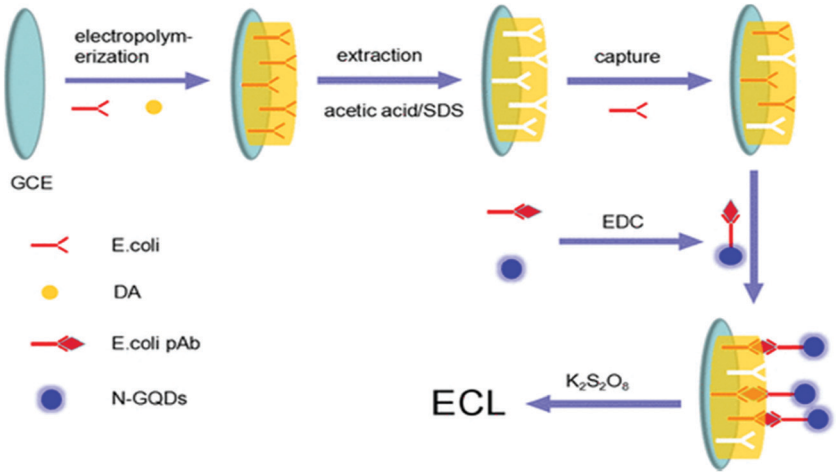

Fig. 12 Schematic representation of the polydopamine-imprinted polymer and N-GQD-based ECL sensing platform toward the quantitative detection of *E. coli* (reproduced with permission from ref. 220, copyright 2017 American Chemical Society).

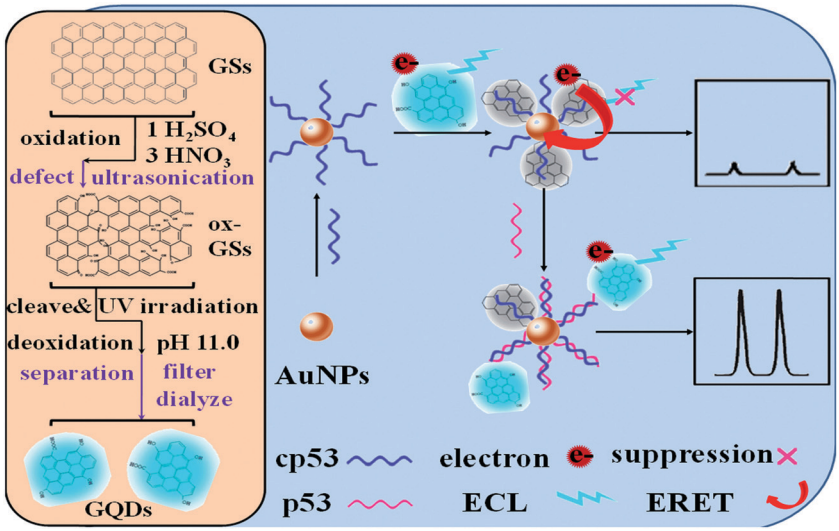

Fig. 13 Pictorial representation of the ECL biosensor based on GQDs (donor) and AuNPs (acceptor) for the detection of DNA damage (reproduced from ref. 210 with permission from Royal Society of Chemistry).

quenched by the ECL-RET from GQDs to nearby AuNPs, while the ECL signal recovered linearly upon the addition of target p53 ssDNA over the detection range of 25–400 nM. Similarly, Liang and their team reported another ECL-RET based biosensor, using GQDs and antibody (anti-phosphoserine)-conjugated GO (Ab-GO) as the donor–acceptor pair to monitor the activity of protein kinase.[211] Yan *et al.* developed a Cu_2O nanosphere and GQDsbased reproducible ECL sensing probe for the effective detection of the pesticide pentachlorophenol (PCP).[212] The as-prepared ECL system exhibited a detection limit of 6.6 pg mL^{-1} within the linear range of 0.02–300 ng mL^{-1}. The incorporation of GQDs enhanced the catalytic performance of the Cu_2O nanospheres owing to their excellent electron-transfer capability. Next, Jie and co-workers deposited GQDs on the poly(diallyldimethylammonium chloride) (PDDA)–GO complex for the development of an efficient ECL biosensor to determine DNA through a cycling amplification approach.[213] Chen *et al.* reported the N-GQDs-based dual-potential (cathodic as well as anodic) single-luminophore ECL platform for the ratiometric detection of Co^{2+} ions.[214] The as-prepared ECL sensor displayed good linearity in the concentration range from 1.0 to 70 μM with a detection limit of 0.2 μM. Wu *et al.* demonstrated the sensitive detection of prostate-specific antigen (PSA) using an electrochemiluminescent immunosensor based on Au/Ag–rGO and functionalized GQDs. Both aminated and carboxylated GQDs were modified on the electrode to provide an improved ECL signal. The proposed biosensor revealed a LOD of 0.29 pg mL^{-1} and the linear dynamic range from 1 pg mL^{-1} to 10 ng mL^{-1} towards PSA detection.[215] Further, Lu *et al.* reported the highly sensitive detection of aflatoxin B1 by fabricating an ECL biosensor based on gold nanorods (AuNRs), GQDs and the poly(indole-6-carboxylic acid)/flower-gold (PICA/F-Au) nanocomposite. The fabricated biosensor exhibited excellent stability, reproducibility, and selectivity with a LOD and linear range of 0.00375 ng mL^{-1} and 0.01–100 ng mL^{-1}, respectively.[216] In another report, Yang *et al.* utilized GQDs as a signal enhancer in the development of an ECL biosensor for direct glucose detection. The presence of GQDs offered direct electron transfer between the electrode surface and GOx. This GOx/GQDs-based biosensor demonstrated exciting sensing characteristics with a broader linear range from 5×10^{-6} to 1.5×10^{-3} mol L^{-1} and a higher sensitivity of 5×10^{-6} mol L^{-1}.[217] Liu and their team demonstrated the detection of AA using an ECL sensing probe based on luminol, and N,S-GQDs as the FRET donor–acceptor pair, respectively. In addition, PEI and PtNPs were utilized as the linker of the FRET pair and the co-reaction accelerator, respectively. It was observed that the ECL intensity of luminol remains constant, whereas the ECL intensity of S-GQDs decreased gradually with increasing AA concentration.[218] Recently, Peng *et al.* employed S,P-GQDs as ECL immunomarkers toward the sensitive quantification of okadaic acid (OA) in shellfish. The co-doping with S and P significantly improved the ECL performance in contrast to the mono-doped GQDs. Besides, the proposed immunosensor revealed exciting sensing parameters including a lower LOD (0.005 ng mL^{-1}) and a wider linear detection range (0.01–20 ng mL^{-1}) for OA detection.[219] The sensing characteristics of different GQDs-based ECL biosensors have been summarized in Table 3.

5.3 Electrochemical biosensors

Electrochemical biosensors are the analytical devices that provide quantitative information on an analyte by converting a biological signal into a final readable electrical signal.[11,25] Over the past two decades, the field of electrochemical biosensing has gained extensive research interest toward the detection of various infectious and non-infectious diseases.[25,223–227] These are essential for point-of-care testing (POCT) due to their exciting characteristics, including high sensitivity, ease of use, disposability, portability, simplicity, and cost-effectiveness.[223,228] The components of these biosensors include a bio-recognition element, an immobilization matrix, and a transducer surface. Recently, GQDs have evolved as an outstanding material for the design of various electrochemical biosensors owing to their outstanding properties such as fast transduction, a high electron-transfer rate, inimitable

Table 3 Summary of different GQD-based ECL biosensors along with their sensing characteristics

Sensing platform	Analyte detected	LOD	Detection range	Ref.
BamHI-GQDs	Hepatitis C virus	0.45 fM	5 fM to 100 pM	207
GQDs-chitosan	Glucose	0.3 pM	1.2–120 pM	208
PDA-SIP-N-GQDs	*E. coli*	8 CFU mL^{-1}	10^1–10^7 CFU mL^{-1}	220
GQDs–AuNPs	p53 DNA damage	13 nM	25–400 nM	210
GQDs and GO	Protein kinase	0.05 U mL^{-1}	0.05–5 U mL^{-1}	211
GQDs-Cu_2O	Pentachlorophenol	6.6 pg mL^{-1}	0.02–300 ng mL^{-1}	221
PDDA-GO-GQDs	DNA	0.1 pM	1.0 pM to 1000 nM	213
N-GQDs	Co^{2+}	0.2 μM	1.0–70 μM	214
GQDs/Au/Ag–rGO	Prostate-specific antigen	0.29 pg mL^{-1}	~1 pg mL^{-1} to ~10 ng mL^{-1}	222
PICA/F-Au/GQDs/AuNRs	Aflatoxin B1	0.00375 ng mL^{-1}	0.01–100 ng mL^{-1}	216
GOx/GQDs	Glucose	5×10^{-6} mol L^{-1}	5×10^{-6} to 1.5×10^{-3} mol L^{-1}	217
NSGQDs-PEI-luminol-Pt	AA	3.3 nM	10–360 nM	218
P,S-GQDs	OA	0.005 ng mL^{-1}	0.01–20 ng mL^{-1}	219

electrocatalytic characteristics, higher surface areas, ease of surface functionalization, and higher biomolecule loading. These GQD-based electrochemical biosensors have been used for the detection of small molecules, nucleic acids, bioflavonoids, amino acids, vitamins, heavy metal ions, and biomarkers with remarkable biosensing characteristics.[229]

Hu *et al.* developed a GQDs-based electrochemical biosensor for the detection of mi-RNA155, wherein GQDs were utilized for the immobilization of horseradish peroxidase (HRP). The as-fabricated biosensor exhibited the highly sensitive detection of mi-RNA155 with a LOD of 0.14 fM and a dynamic range of 1 fM to 100 pM owing to the excellent compatibility and the higher surface-to-volume ratio of the GQDs.[127] Rezei *et al.* demonstrated an electrochemical-sensing platform for H_2O_2 quantification by immobilizing hemoglobin (Hb) on a GQDs–chitosan nanocomposite. This Hb-GQDs–Chit-based biosensor revealed remarkable biosensing characteristics, including a remarkable LOD (0.68 μM), a high sensitivity (0.53 μA μM^{-1} cm^{-2}), a wider detection range (1.5–195 μM), and an improved heterogeneous electron-transfer rate. The excellent sensing characteristics of the designed biosensor were ascribed to the high surface area, and unique electron-transfer ability of the GQDs.[230] Tuteja *et al.*[231] demonstrated a GQDs-deposited screen-printed electrode (SPE)-based efficient biosensor toward the identification of cardiac marker myoglobin (cMyo). The developed biosensor (Ab/GQDs/SPE) utilized electrochemical impedance spectroscopy (EIS) for cMyo detection and exhibited a linear correlation between impedance and antigen concentration ranging from 0.01 to 100 ng mL^{-1}. GQDs provided a fast heterogeneous electron-transfer rate and an improved biomolecule loading owing to their larger surface area. Similarly, Vasilescu *et al.* modified the SPE with a nanocomposite of molybdenum disulphide and GQDs. These modified electrodes were immobilized with the laccase enzyme, and the analytical response for the detection of caffeic acid was measured through chronoamperometry. The synergetic effect of the GQDs–MoS_2 nanocomposite provided high conductivity, a large surface area, and the good electrocatalytic activity required for the fabrication of an efficient biosensor. The fabricated biosensor exhibited significant biosensing parameters, including a sensitivity of 17.92 nA μM^{-1}, and a LOD of 0.32 μM over a concentration range of 0.38–100 μM.[232] Xi *et al.* described the electrochemical biosensor based on palladium (Pd) nanoparticle-loaded N-GQDs and N-doped carbon hollow nanospheres (HNS) toward H_2O_2 determination (Fig. 14). This hybrid nanomaterial-based biosensor revealed excellent sensing characteristics, including a low LOD, high stability, selectivity, reproducibility, and sensitivity as well as a fast response time towards the real-time detection of normal and treated (radiotherapy and chemotherapy) cancer cells. The improved sensing characteristics and electrocatalytic activity were attributed to the synergistic effect of the PdNPs and N-GQDs. Specifically, the N-GQDs offered fast heterogeneous electron transfer and excellent peroxidase mimetic activity.[233] Similarly, Li *et al.* demonstrated a ternary GQDs–PNF–GO nanohybrid-based electrochemical biosensor for H_2O_2 detection that revealed high selectivity, sensitivity, a low detection limit, and a wide linear range.[234] Another efficient aptasensor based on the AgNPs/thiol-GQDs nanocomposite was designed by Roushani and colleagues towards the detection of 2,4,6-trinitrotoluene (TNT). The presence of GQDs offers a higher surface-to-volume ratio that provided increased loading of the TNT-binding aptamer.[235] The advantages of this strategy may be extended to other nanoparticles and probable hopeful implications in the

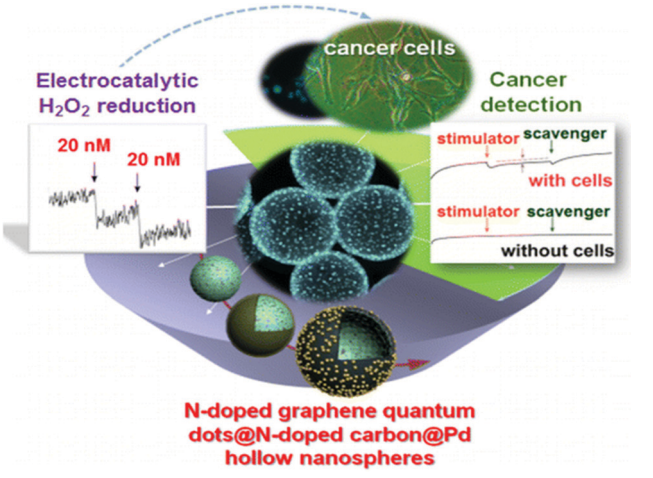

Fig. 14 GQD-based electrochemical biosensors based on palladium (Pd) nanoparticle-loaded N-GQDs and N-doped carbon hollow nanospheres (HNS) for H_2O_2 detection in cancer cells (reproduced with permission from ref. 237, copyright 2016 American Chemical Society).

design of various electrochemical biosensors for target analyte detection. Huang *et al.* described the detection of DA (Fig. 15) in both live PC_{12} cells and serum samples *via* the use of the MWCNT-GQDs nanocomposite as the sensing platform, and revealed a LOD of 0.87 nM. The GQDs provided the anionic groups, which attracted the cationic DA *via* π–π superposition interactions, thereby enabling the selective determination of DA.[236]

In another study, Arumugasamy and co-workers also reported the MWCNT–GQDs nanocomposite for DA detection employing the DPV technique. This nanocomposite-based biosensor revealed noteworthy electrocatalytic activity for DA oxidation in standard as well as spiked samples with LOD values of 95 nM and 110 nM, respectively, over a linear correlation range of 0.25–μM.[238] Gogola *et al.* employed GQDs as a support material for aptamer immobilization as well as an electrochemical signal amplifier toward the label-free detection of p24-human immunodeficiency virus (HIV) protein. Under optimized conditions, this aptasensor exhibited a LOD of 51.7 pg mL^{-1} over the dynamic range from 0.93 ng mL^{-1} to 93 μg mL^{-1}.[239] Cai *et al.* established an electrochemical sensing platform utilizing polyaniline (PANI)-functionalized GQDs toward the quantification of cardiac disease biomarkers. The presence of GQDs provided faster electron-transfer kinetics, enabling the sensitive detection of calycosin. The as-fabricated biosensor revealed a LOD of 9.8×10^{-6} mol L^{-1} over the detection range of 1.1×10^{-5} to 3.52×10^{-4} mol L^{-1}.[240] GQDs have also been used in the fabrication of electrochemical biosensors for quantifying several metal ions in food samples and the biological environment. In line with this, Lu and colleagues developed a nanochannel-confined GQDs-based ultrasensitive biosensor for the detection of Cd^{2+}, Cu^{2+}, and Hg^{2+} ions (Fig. 16A) with a LOD of 4.3 nM, 8.3 pM, and 9.8 pM, respectively. GQDs worked as the signal amplifier and recognition element by interacting with the target ions to provide faster charge transfer and selective enrichment of the analytes.[241] Recently, Sun *et al.* demonstrated a sensitive immunosensor for heat shock protein 70 (HSP70) (depression marker) using PANI-functionalized GQDs (PANI-GQDs) as the sensing material. Owing to the excellent structure, better bioactivity, and large surface-to-volume ratio of the PANI-GQDs, the immunosensor revealed exciting biosensing characteristics, including a lower LOD (0.05 ng mL^{-1}) and a broader linear correlation 0.0976–100 ng mL^{-1}.[242] More recently, Soleimanian *et al.* reported the sensitive detection of the CD123 marker in leukemia cells by fabricating a GQDs-based cytosensor. The larger surface area of the GQDs enables increased biotinylated antibody immobilization, leading to the improved sensitivity of the cytosensor. This GQDs-enabled cytosensor exhibited a LOD of 1 cell per mL with a dynamic range of 1–25 cells per mL.[243] Further, Ozcan *et al.* reported the electrochemical detection of IL-6 using the molecularly imprinted composite of GQDs and MWCNTs (GQDs/f-MWCNTs). The GQDs/f-MWCNTs provided a higher surface area and prevented the aggregation of GQDs, resulting in a higher sensitivity, good electrocatalytic activity, and faster charge-transfer kinetics. The as-fabricated biosensor exhibited a LOD of 0.0030 pg mL^{-1} in the detection range of 0.01–2.0 pg mL^{-1}.[244] Bhardwaj *et al.* reported the sensitive detection of aflatoxin B1 (AFB1) utilizing GQDs-decorated molybdenum disulfide (MoS_2) nanosheets as the electrode material in the detection range of 0.1–3.0 ng mL^{-1} and a LOD of 0.09 ng mL^{-1}. The conjugation of GQDs with MoS_2 nanosheets offered a higher electrocatalytic activity, improved electrical conductivity, large surface area, and abundant exposed edge sites.[245] Recently, Mahmoudi and their team demonstrated an

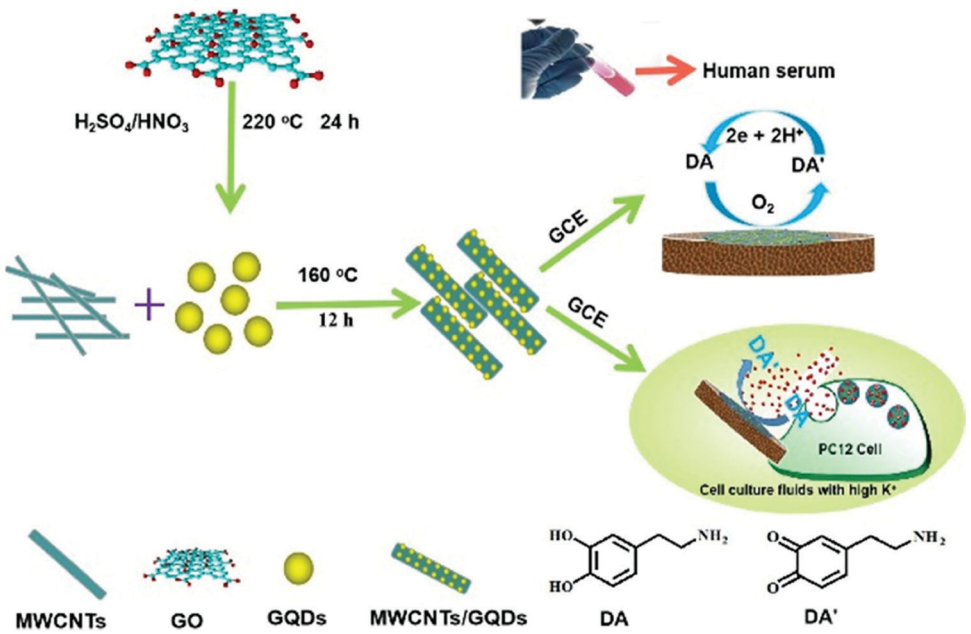

Fig. 15 GQDs/MWCNT based electrochemical biosensor for DA detection in live PC_{12} cells and serum samples (reproduced with permission from ref. 236, copyright 2020 American Chemical Society).

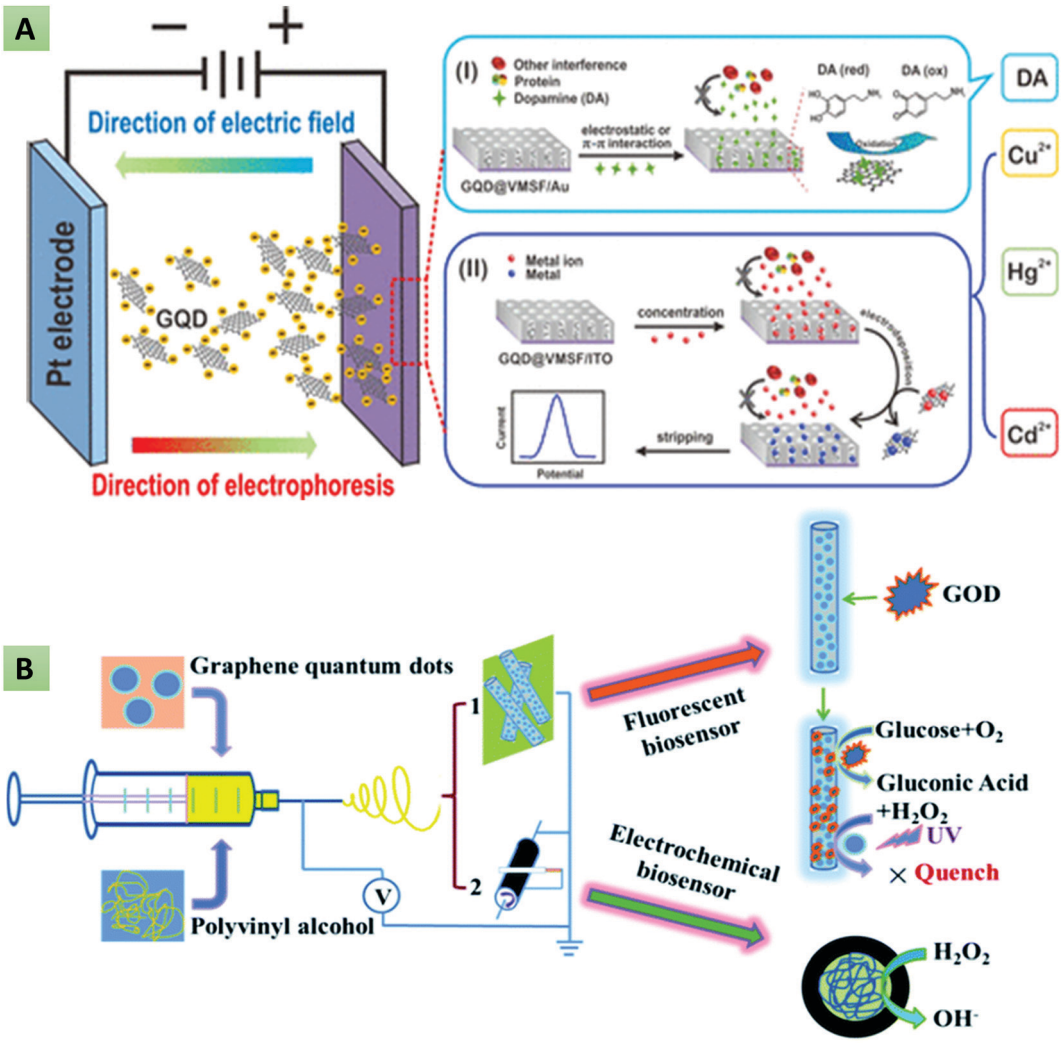

Fig. 16 (A) Electrophoretic deposition of GQD@mesoporous silica-nanochannel film (VMSF) on the electrode surface for the detection of Cd^{2+}, Cu^{2+}, and Hg^{2+} ions (reproduced with permission from ref. 241, copyright 2018 American Chemical Society). (B) Glucose detection based on an electrospun GQDs/PVA nanofibrous membrane (reproduced from ref. 254 with permission from Royal Society of Chemistry).

electrochemical sensing platform based on GQDs and an IL-modified carbon paste electrode (CPE) toward topotecan detection and exhibited a LOD of 0.1 μM in the detection range of 0.35–100.0 μM.[246] Ashraf *et al.* reported an ultrasensitive electrochemical biosensor for bisphenol A (BPA) detection in live cells based on single-crystal Cu_2O nanostructures with GQDs on their surface (Cu_2O–CuO@GQDs). Owing to the mixed copper valences, exposed Cu(111) crystallographic planes, enhanced redox reaction kinetics, and boosted surface area in view of synergistic effects, the proposed sensing platform exhibited a high sensitivity (636 μA mM^{-1} cm^{-2}), a wide linear range (2 nM to 11 mM), and a low LOD ($\leq$1 nM).[247] Arab *et al.* demonstrated the sensitive analysis of 4-aminophenol and paracetamol utilizing a MWCNT and GQDs-based electrochemical biosensing platform and exhibited a LOD of 0.017 μmol L^{-1} and 0.010 μmol L^{-1} for 4-aminophenol and paracetamol, respectively.[248] Similarly, Ghanbari *et al.* demonstrated HCV detection using specific aptamer-functionalized GQDs with a LOD of 3.3 pg mL^{-1}.[249] GQDs possess multiple hydrophobic planes and hydrophilic edges that served as substrates for the immobilization of aptamers through π–π stacking interactions. Later, the same researchers reported an aptasensor based on AuNPs and thiolated GQDs (GQDs-SH) for detecting streptomycin *via* the EIS technique and revealed a wide dynamic range of 0.1–700 pg mL^{-1}.[250] Gupta and co-workers reported the electrochemical detection of ochratoxin-A utilizing GQD-decorated zirconia nanoflowers (GQDs@ZrO_2) in the detection range of 1–20 ng mL^{-1}. The decoration of GQDs on ZrO_2 provided enhanced biosensing characteristics and a higher biomolecule loading owing to the superior electrical conductivity and higher surface area of the GQDs.[251] Further, Yang and co-workers described the functionalized N-GQDs (PtPd/N-GQDs@Au)-based label-free electrochemical biosensor toward the sensitive determination of carcinoembryonic antigen (CEA). The proposed biosensor revealed an extreme LOD of 2 fg mL^{-1} over the dynamic range of 5 fg mL^{-1} to 50 ng mL^{-1}.[252] More recently, another study by Gangaboina *et al.* reported the detection of CEA utilizing N,S-GQDs-decorated Au–PANI nanowires, revealing a LOD of 0.01 ng mL^{-1} over the dynamic range of

Table 4 Summary of different GQD-based electrochemical biosensors along with their sensing characteristics

Sensing platform	Analyte detected	Sensitivity	LOD	Time (min)	Detection range	Ref.
GQDs-HRP	miRNA-155	—	0.14 fM	60	1 fM to 100 pM	127
Hb-GQDs-Chit	H_2O_2	0.53 A M^{-1} cm^{-2}	0.68 μM	0.08	1.5–195 μM	230
GQDs-SPE	Myoglobin		0.01 ng mL^{-1}	—	0.01–100 ng mL^{-1}	255
MoS_2-GQDs	Caffeic acid	17.92 nA μM^{-1}	0.32 μM	—	0.38–100 μM	256
Pd–N-GQDs–HNS	H_2O_2	0.59 mA cm^{-2} mM^{-1}	20 nM	240	0–5 mM	237
GQDs–PNF–GO	H_2O_2	—	0.055×10^{-6} M		0.01×10^{-3} to 7.2×10^{-3} M	257
AgNPs/thiol-GQDs	Trinitrotoluene	—	3.33×10^{-7}	35	1.00×10^{-6} to 3.00×10^{4}	235
MWCNT-GQDs	DA	—	0.87 nM	—	0.005–100.0 μM	236
MWCNT-GQDs	DA	—	0.095 μM	—	0.25–250 μM	238
GQDs	p24-HIV	1.293 μA dec^{-1}	51.7 pg mL^{-1}		0.93 ng mL^{-1} to 93 μg mL^{-1}	239
PANI-GQDs	Calycosin	—	9.8×10^{-6} mol L^{-1}	3	1.1×10^{-5} to 3.52×10^{-4} mol L^{-1}	240
VMSF-GQDs	Hg^{2+}, Cu^{2+}, Cd^{2+}, and DA	51.2 μA nM^{-1}	9.8 pM, 8.3 pM, 4.3 nM, and 120 nM		10 pM to 1.0 nM 10 pM to 1.0 nM 20.0 nM to 1.0 μM 200 nM to 20 μM	241
GQDs/f-MWCNTs	Interleukin-6	—	0.0030 pg mL^{-1}	15	0.01–2.0 pg mL^{-1}	244
PANI-GQDs	HSP70		0.05 ng mL^{-1}	30	0.0976–100 ng mL^{-1}	242
GQDs-AuNPs	CD123	—	1 cell per mL	–	1–25 cells per mL	243
GQDs-MoS_2	Aflatoxin B1	44.44 Ω (ng mL^{-1})$^{-1}$ cm^{-2}	0.09 ng mL^{-1}		0.1–3.0 ng mL^{-1}	245
GQDs-CPE	Topotecan	—	0.1 μM	5	0.35–100.0 μM	246
Cu_2O–CuO@GQDs	BPA	636 μA mM^{-1} cm^{-2}	≤1 nM	–	2 nM to11 mM	247
GQDs-GCE	Hepatitis C virus (HCV)	—	3.3 pg mL^{-1}	40	10–400 pg mL^{-1}	249
AuNPs/GQD-SH	Streptomycin	—	0.033 pg mL^{-1}	120	0.1–700 pg mL^{-1}	250
GQDs@ZrO_2	Ochratoxin A	5.62 μA mL ng^{-1} cm^{-2}	0.38 ng mL^{-1}	15	1–20 ng mL^{-1}	251
PtPd/N-GQDs@Au	Carcino-embryonic antigen (CEA)		2 fg mL^{-1}		5 fg mL^{-1} to 50 ng mL^{-1}	252
N,S-GQDs/Au-PANI	CEA	—	0.01 ng mL^{-1}	—	0.5–1000 ng mL^{-1}	258
AgNPs/GQD-SH	HCV		3 fg mL^{-1}	30	0.05 pg mL^{-1} to 60 ng mL^{-1}	234

0.5–1000 ng mL^{-1}.[253] The highly sensitive detection of CEA was primarily ascribed to the excellent electro-conductivity of the N,S-GQDs that provided the faster electron-transfer kinetics. Zhang *et al.* described the fabrication of a glucose biosensor (Fig. 16B) based on electrospun GQDs and polyvinyl alcohol (GQDs/PVA) nanofibrous membrane.[254] Further, Valipour *et al.* reported the nanocomposite of Ag nanoparticles and thiolated GQDs (AgNPs/GQDs-SH) in fabricating a highly sensitive immunosensor for the detection of HCV, exhibiting remarkable sensing parameters including a lower LOD (3 fg mL^{-1}) and a broad linear detection range (0.05 pg mL^{-1} to 60 ng mL^{-1}).[234] The remarkable performance of the designed biosensor was ascribed to the higher surface area and the electronic structure of GQDs-SH that provided the higher electrocatalytic activity. Table 4 summarizes the different GQD-based electrochemical biosensors along with their sensing characteristics including the sensitivity, LOD, response time, and linear detection range.

6. Summary and future prospects

Over the past decade, GQDs has emerged as an indispensable material because of their outstanding properties of chemical stability, desirable aqueous solubility, an abundance of active sites, excellent biocompatibility, tunable photoluminescence, fast transduction rate, the capability of direct electron transfer, electrocatalytic activity, larger surface areas and ease of surface functionalization. GQDs have been surface-functionalized with a variety of biomolecules, including proteins, enzymes, and oligonucleotides, towards the fabrication of optical and electrochemical biosensing platforms. In this review, the recent progress related to bottom-up (cage opening, incomplete carbonization, thermal pyrolysis, microwave, and hydrothermal processes) and top-down (oxygen cutting, physical grinding, hydrothermal/solvothermal methods, reductive cutting, electrochemical methods, *etc.*) synthesis strategies, optical and electrochemical properties as well as their regulation through heteroatom doping and surface functionalization have been discussed. Further efforts have been made to enlighten the scope of GQDs in the fabrication of numerous optical and electrochemical biosensors toward the quantification of nucleic acids, bioflavonoids, amino acids, vitamins, heavy metal ions, biomarkers, and other small molecules. Despite tremendous progress, there are still some challenges that need to be resolved. For instance, the mass-scale production of GQDs has not yet been achieved. The currently described methods permit limited production with a wide range of heterogeneity in size, shape, and properties. In addition, the GQDs prepared for a specific application might not be suitable for other desired applications. This is a major drawback while shifting from bench to real-world applications since the production procedure tends to be tedious. Additionally, the biofouling characteristics, reproducibility of the synthesis procedures, and storage stability are some of the points that have not yet been evaluated in detail. Therefore, researchers are engrossed in developing a green and cost-effective synthetic techniques, which, along with maintaining the uniformity in size and excellence in properties, would result in large-scale production. Since GQDs exhibit both excitation-dependent and excitation-independent emission spectra, another important challenge related to the mechanism behind their

inherent photoluminescence properties still requires further theoretical and experimental investigations. Moreover, only a few studies have discussed the mechanism of electron transfer and enhancement in the quantum yield due to heteroatom doping and surface functionalization. Therefore, in the near future, in-depth investigations of these issues will certainly assist researchers and scientists in understanding the optoelectronic characteristics of GQDs, which will open a new window towards the development of highly efficient biosensing platforms.

Conflicts of interest

There are no conflicts to declare.

Acknowledgements

The current work is supported by the Department of Biotechnology (No. BT/PR25095/NER/95/1011/2017), Government of India. G. P. is thankful to the Department of Science and Technology (DST), Government of India, Technology Innovation Hub (TIH) for Devices Materials and Technology Foundation, IIT Roorkee [A Section-8 Company: Divyasampark IHub for Devices Materials and Technology Foundation]. A. K. is thankful to the Ministry of Education, Government of India, for the PhD fellowship. S. K. is grateful to DST, Government of India, for providing the SERB-OVDF fellowship.

References

1 J. Wen, Y. Xu, H. Li, A. Lu and S. Sun, *Chem. Commun.*, 2015, **51**, 11346–11358.
2 P. Allawadhi, A. Khurana, S. Allwadhi, K. Joshi, G. Packirisamy and K. K. Bharani, *Nano Today*, 2020, **35**, 100982.
3 A. Khurana, P. Anchi, P. Allawadhi, V. Kumar, N. Sayed, G. Packirisamy and C. Godugu, *Nanomedicine*, 2019, **14**, 1805–1825.
4 A. Khurana, P. Anchi, P. Allawadhi, V. Kumar, N. Sayed, G. Packirisamy and C. Godugu, *Nanomedicine*, 2019, **18**, 54–65.
5 A. Kalkal, S. Kumar, P. Kumar, R. Pradhan, M. Willander, G. Packirisamy, S. Kumar and B. D. Malhotra, *Addit. Manuf.*, 2021, **46**, 102088.
6 S. Kumar, J. Kumar and S. N. Sharma, *Optik*, 2020, **208**, 164540.
7 Ashish, N. Ahmad, P. Gopinath and A. Vinogradov, in *3D Printing Technology in Nanomedicine*, ed. N. Ahmad, P. Gopinath and R. Dutta, Elsevier, 2019, pp. 1–22, DOI: 10.1016/B978-0-12-815890-6.00001-3.
8 S. Kumar and A. Kalkal, in *Nanotechnology in Cancer Management*, ed. K. R. Khondakar and A. K. Kaushik, Elsevier, 2021, pp. 43–71, DOI: 10.1016/B978-0-12-818154-6.00008-1.
9 S. Kumar, Ashish, S. Kumar, S. Augustine, S. Yadav, B. K. Yadav, R. P. Chauhan, A. K. Dewan and B. D. Malhotra, *Biosens. Bioelectron.*, 2018, **102**, 247–255.
10 S. Augustine, P. Kumar and B. D. Malhotra, *ACS Appl. Bio Mater.*, 2019, **2**, 5366–5378.
11 S. Kumar, J. Kumar and S. N. Sharma, *Mater. Res. Express*, 2018, **5**, 125405.
12 R. Xie, Z. Wang, W. Zhou, Y. Liu, L. Fan, Y. Li and X. Li, *Anal. Methods*, 2016, **8**, 4001–4016.
13 S. Kadian, G. Manik, N. Das, P. Nehra, R. P. Chauhan and P. Roy, *J. Mater. Chem. B*, 2020, **8**, 3028–3037.
14 F. Faridbod and A. L. Sanati, *Curr. Anal. Chem.*, 2019, **15**, 103–123.
15 S. Zhu, Y. Song, X. Zhao, J. Shao, J. Zhang and B. Yang, *Nano Res.*, 2015, **8**, 355–381.
16 A. Kalkal, P. Allawadhi, R. Pradhan, A. Khurana, K. K. Bharani and G. Packirisamy, *Sens. Int.*, 2021, **2**, 100102.
17 S. Kumar, J. Kumar, S. Narayan Sharma and S. Srivastava, *Optik*, 2019, **178**, 411–421.
18 S. Kadian, S. K. Sethi and G. Manik, *Mater. Chem. Front.*, 2021, **5**, 627–658.
19 X. Zhao, W. Gao, H. Zhang, X. Qiu and Y. Luo, in *Handbook of Nanomaterials in Analytical Chemistry*, ed. C. Mustansar Hussain, Elsevier, 2020, pp. 493–505, DOI: 10.1016/B978-0-12-816699-4.00020-7.
20 S. Kadian, G. Manik, A. Kalkal, M. Singh and R. P. Chauhan, *Nanotechnology*, 2019, **30**, 435704.
21 X. T. Zheng, A. Ananthanarayanan, K. Q. Luo and P. Chen, *Small*, 2015, **11**, 1620–1636.
22 B. D. Mansuriya and Z. Altintas, *Sensors*, 2020, **20**, 1072.
23 S. Kadian, B. D. Arya, S. Kumar, S. N. Sharma, R. P. Chauhan, A. Srivastava, P. Chandra and S. P. Singh, *Electroanalysis*, 2018, **30**, 2793–2802.
24 C. Zhao, X. Song, Y. Liu, Y. Fu, L. Ye, N. Wang, F. Wang, L. Li, M. Mohammadniaei and M. Zhang, *J. Nanobiotechnol.*, 2020, **18**, 1–32.
25 R. Pradhan, A. Kalkal, S. Jindal, G. Packirisamy and S. Manhas, *RSC Adv.*, 2021, **11**, 798–806.
26 Z. Fan, S. Li, F. Yuan and L. Fan, *RSC Adv.*, 2015, **5**, 19773–19789.
27 A. Kalkal, R. Pradhan, S. Kadian, G. Manik and G. Packirisamy, *ACS Appl. Bio Mater.*, 2020, **3**, 4922–4932.
28 S. Kumar, T. Vats, S. N. Sharma and J. Kumar, *Optik*, 2018, **171**, 492–500.
29 M. J. Sweetman, S. M. Hickey, D. A. Brooks, J. D. Hayball and S. E. Plush, *Adv. Funct. Mater.*, 2019, **29**, 1808740.
30 D. Iannazzo, A. Pistone, S. Ferro, L. De Luca, A. M. Monforte, R. Romeo, M. R. Buemi and C. Pannecouque, *Bioconjugate Chem.*, 2018, **29**, 3084–3093.
31 S. Gu, C.-T. Hsieh, Y.-M. Chiang, D.-Y. Tzou, Y.-F. Chen and Y. A. Gandomi, *Mater. Chem. Phys.*, 2018, **215**, 104–111.
32 H. Ding, F. Zhang, C. Zhao, Y. Lv, G. Ma, W. Wei and Z. Tian, *ACS Appl. Mater. Interfaces*, 2017, **9**, 27396–27401.
33 N. Wang, L. Li, N. Zhou and S. Chen, *Phys. Status Solidi B*, 2018, **255**, 1700535.
34 R. Ye, C. Xiang, J. Lin, Z. Peng, K. Huang, Z. Yan, N. P. Cook, E. L. G. Samuel, C.-C. Hwang, G. Ruan, G. Ceriotti, A.-R. O. Raji, A. A. Martí and J. M. Tour, *Nat. Commun.*, 2013, **4**, 2943.

35 Y. Dong, C. Chen, X. Zheng, L. Gao, Z. Cui, H. Yang, C. Guo, Y. Chi and C. M. Li, *J. Mater. Chem.*, 2012, **22**, 8764–8766.
36 S. Zhang, L. Sui, H. Dong, W. He, L. Dong and L. Yu, *ACS Appl. Mater. Interfaces*, 2018, **10**, 12983–12991.
37 S. Maiti, S. Kundu, C. N. Roy, T. K. Das and A. Saha, *Langmuir*, 2017, **33**, 14634–14642.
38 Q. Liu, J. Zhang, H. He, G. Huang, B. Xing, J. Jia and C. Zhang, *Nanomaterials*, 2018, **8**, 844.
39 Q. Lu, C. Wu, D. Liu, H. Wang, W. Su, H. Li, Y. Zhang and S. Yao, *Green Chem.*, 2017, **19**, 900–904.
40 A. Halder, M. Godoy-Gallardo, J. Ashley, X. Feng, T. Zhou, L. Hosta-Rigau and Y. Sun, *ACS Appl. Bio Mater.*, 2018, **1**, 452–461.
41 G. Rajender and P. K. Giri, *J. Mater. Chem. C*, 2016, **4**, 10852–10865.
42 B. Liu, J. Xie, H. Ma, X. Zhang, Y. Pan, J. Lv, H. Ge, N. Ren, H. Su and X. Xie, *Small*, 2017, **13**, 1601001.
43 H. Teymourinia, M. Salavati-Niasari, O. Amiri and M. Farangi, *J. Mol. Liq.*, 2018, **251**, 267–272.
44 H. Teymourinia, M. Salavati-Niasari, O. Amiri and H. Safardoust-Hojaghan, *J. Mol. Liq.*, 2017, **242**, 447–455.
45 X. Chu, P. Dai, S. Liang, A. Bhattacharya, Y. Dong and M. Epifani, *Phys. E*, 2019, **106**, 326–333.
46 D. Pan, J. Zhang, Z. Li and M. Wu, *Adv. Mater.*, 2010, **22**, 734–738.
47 D. Pan, L. Guo, J. Zhang, C. Xi, Q. Xue, H. Huang, J. Li, Z. Zhang, W. Yu, Z. Chen, Z. Li and M. Wu, *J. Mater. Chem.*, 2012, **22**, 3314–3318.
48 S. Shen, J. Wang, Z. Wu, Z. Du, Z. Tang and J. Yang, *Nanomaterials*, 2020, **10**, 375.
49 S. Moghimian and P. Sangpour, *J. Appl. Electrochem.*, 2020, **50**, 71–79.
50 M. Vandana, H. Vijeth, S. P. Ashokkumar and H. Devendrappa, *Inorg. Chem. Commun.*, 2020, **117**, 107941.
51 F. Behzadi, E. Saievar-Iranizad and A. Bayat, *Mater. Res. Express*, 2019, **6**, 105615.
52 Z. Fan, Y. Nie, Y. Wei, J. Zhao, X. Liao and J. Zhang, *Mater. Sci. Eng.*, 2019, **103**, 109824.
53 Y. Shin, J. Park, D. Hyun, J. Yang, J.-H. Lee, J.-H. Kim and H. Lee, *Nanoscale*, 2015, **7**, 5633–5637.
54 X. Wu, L. Ma, S. Sun, K. Jiang, L. Zhang, Y. Wang, H. Zeng and H. Lin, *Nanoscale*, 2018, **10**, 1532–1539.
55 P. Luo, X. Guan, Y. Yu, X. Li and F. Yan, *Nanomaterials*, 2019, **9**, 201.
56 D. Huang, M. Zeng, L. Wang, L. Zhang and Z. Cheng, *RSC Adv.*, 2018, **8**, 34839–34847.
57 S. Pourhashem, E. Ghasemy, A. Rashidi and M. R. Vaezi, *J. Coat. Technol. Res.*, 2020, **17**, 19–55.
58 B. Oh and C. H. Lee, *Pharm. Res.*, 2016, **33**, 2736–2747.
59 J.-H. Zhang, T. Sun, A. Niu, Y.-M. Tang, S. Deng, W. Luo, Q. Xu, D. Wei and D.-S. Pei, *Biomaterials*, 2017, **133**, 49–59.
60 Z. Wang, J. Yu, X. Zhang, N. Li, B. Liu, Y. Li, Y. Wang, W. Wang, Y. Li and L. Zhang, *ACS Appl. Mater. Interfaces*, 2016, **8**, 1434–1439.
61 H. Gao, C. Xue, G. Hu and K. Zhu, *Ultrason. Sonochem.*, 2017, **37**, 120–127.
62 L. Lu, Y. Zhu, C. Shi and Y. T. Pei, *Carbon*, 2016, **109**, 373–383.
63 X. Zhou, Y. Zhang, C. Wang, X. Wu, Y. Yang, B. Zheng, H. Wu, S. Guo and J. Zhang, *ACS Nano*, 2012, **6**, 6592–6599.
64 L. Lin and S. Zhang, *Chem. Commun.*, 2012, **48**, 10177–10179.
65 S. Karmakar, T. K. Das, S. Kundu, S. Maiti and A. Saha, *J. Indian Chem. Soc.*, 2021, 100069, DOI: 10.1016/j.jics.2021.100069.
66 H. Huang, S. Yang, Q. Li, Y. Yang, G. Wang, X. You, B. Mao, H. Wang, Y. Ma, P. He, Z. Liu, G. Ding and X. Xie, *Langmuir*, 2018, **34**, 250–258.
67 L. Chen, C. Wu, P. Du, X. Feng, P. Wu and C. Cai, *Talanta*, 2017, **164**, 100–109.
68 Y. Li, S. Li, Y. Wang, J. Wang, H. Liu, X. Liu, L. Wang, X. Liu, W. Xue and N. Ma, *Phys. Chem. Chem. Phys.*, 2017, **19**, 11631–11638.
69 H. Kalita, V. S. Palaparthy, M. S. Baghini and M. Aslam, *Carbon*, 2020, **165**, 9–17.
70 S. Ahirwar, S. Mallick and D. Bahadur, *ACS Omega*, 2017, **2**, 8343–8353.
71 Y. Yan, H. Li, Q. Wang, H. Mao and W. Kun, *J. Mater. Chem. C*, 2017, **5**, 6092–6100.
72 X. Yan, X. Cui, B. Li and L.-S. Li, *Nano Lett.*, 2010, **10**, 1869–1873.
73 X. Yan, X. Cui and L.-S. Li, *J. Am. Chem. Soc.*, 2010, **132**, 5944–5945.
74 D. Liu, X. Chen, Y. Hu, T. Sun, Z. Song, Y. Zheng, Y. Cao, Z. Cai, M. Cao and L. Peng, *Nat. Commun.*, 2018, **9**, 1–10.
75 T. Lin, K. Chih, C. Yuan, J. Shen, C. Lin and W. Liu, *Nanoscale*, 2015, **7**, 2708–2715.
76 M. Sajjad, V. Makarov, M. Sultan, W. Jadwisienczak, B. Weiner and G. Morell, *Adv. Mater. Sci. Eng.*, 2018, **2018**, 3254081.
77 M. J. Deka and D. Chowdhury, *ChemistrySelect*, 2017, **2**, 1999–2005.
78 S. Kumar, S. K. T. Aziz, O. Girshevitz and G. D. Nessim, *J. Phys. Chem. C*, 2018, **122**, 2343–2349.
79 S. R. M. Santiago, T. N. Lin, C. T. Yuan, J. L. Shen, H. Y. Huang and C. A. J. Lin, *Phys. Chem. Chem. Phys.*, 2016, **18**, 22599–22605.
80 S. R. M. Santiago, T. N. Lin, C. H. Chang, Y. A. Wong, C. A. J. Lin, C. T. Yuan and J. L. Shen, *Phys. Chem. Chem. Phys.*, 2017, **19**, 22395–22400.
81 S. Kang, Y. K. Jeong, K. H. Jung, Y. Son, W. R. Kim, J. H. Ryu and K. M. Kim, *Opt. Express*, 2020, **28**, 21659–21667.
82 S. Gu, C.-T. Hsieh, Y.-Y. Tsai, Y. Ashraf Gandomi, S. Yeom, K. D. Kihm, C.-C. Fu and R.-S. Juang, *ACS Appl. Nano Mater.*, 2019, **2**, 790–798.
83 C. K. Chua, Z. Sofer, P. Šimek, O. Jankovský, K. Klímová, S. Bakardjieva, Š. Hrdličková Kučková and M. Pumera, *ACS Nano*, 2015, **9**, 2548–2555.
84 S. Kadian and G. Manik, *Luminescence*, 2020, **35**, 763–772.
85 Y. Sheng, W. Dai, J. Gao, H. Li, W. Tan, J. Wang, L. Deng and Y. Kong, *Mater. Sci. Eng.*, 2020, **112**, 110888.

86 J. Tian, W. Wei, J. Wang, S. Ji, G. Chen and J. Lu, *Anal. Chim. Acta*, 2018, **1000**, 265–272.
87 Q. Feng, W. Xiao, Y. Liu, Y. Zheng, Y. Lin, J. Li, Q. Ye and Z. Huang, *Materials*, 2018, **11**, 1166.
88 S. Li, S. Zhou, Y. Li, X. Li, J. Zhu, L. Fan and S. Yang, *ACS Appl. Mater. Interfaces*, 2020, **12**, 27819–27820.
89 Y. Dong, J. Shao, C. Chen, H. Li, R. Wang, Y. Chi, X. Lin and G. Chen, *Carbon*, 2012, **50**, 4738–4743.
90 T. Dey, S. Mukherjee, A. Ghorai, S. Das and S. K. Ray, *Carbon*, 2018, **140**, 394–403.
91 M. T. Hasan, R. Gonzalez-Rodriguez, C. Ryan, N. Faerber, J. L. Coffer and A. V. Naumov, *Adv. Funct. Mater.*, 2018, **28**, 1804337.
92 M. Shehab, S. Ebrahim and M. Soliman, *J. Lumin.*, 2017, **184**, 110–116.
93 D. Qu, M. Zheng, P. Du, Y. Zhou, L. Zhang, D. Li, H. Tan, Z. Zhao, Z. Xie and Z. Sun, *Nanoscale*, 2013, **5**, 12272–12277.
94 C. Zhang, Y. Cui, L. Song, X. Liu and Z. Hu, *Talanta*, 2016, **150**, 54–60.
95 R. Zhang, J. R. Adsetts, Y. Nie, X. Sun and Z. Ding, *Carbon*, 2018, **129**, 45–53.
96 R. Liu, D. Wu, X. Feng and K. Müllen, *J. Am. Chem. Soc.*, 2011, **133**, 15221–15223.
97 L. Tang, R. Ji, X. Cao, J. Lin, H. Jiang, X. Li, K. S. Teng, C. M. Luk, S. Zeng, J. Hao and S. P. Lau, *ACS Nano*, 2012, **6**, 5102–5110.
98 S. Gu, C.-T. Hsieh, C.-Y. Yuan, Y. Ashraf Gandomi, J.-K. Chang, C.-C. Fu, J.-W. Yang and R.-S. Juang, *J. Lumin.*, 2020, **217**, 116774.
99 N. E. Lee, S. Y. Lee, H. S. Lim, S. H. Yoo and S. O. Cho, *Nanomaterials*, 2020, **10**, 277.
100 Y. Ping, L. Ruiyi, Y. Yongqiang, L. Zaijun, G. Zhiguo, W. Guangli and L. Junkang, *Spectrochim. Acta, Part A*, 2018, **203**, 139–146.
101 G.-L. Hong, H.-L. Zhao, H.-H. Deng, H.-J. Yang, H.-P. Peng, Y.-H. Liu and W. Chen, *Int. J. Nanomed.*, 2018, **13**, 4807–4815.
102 S. Li, S. Zhou, Y. Li, X. Li, J. Zhu, L. Fan and S. Yang, *ACS Appl. Mater. Interfaces*, 2017, **9**, 22332–22341.
103 H. Rasuli, R. Rasuli, M. Alizadeh and G. BoonTong, *Results Phys.*, 2020, **18**, 103200.
104 A. Abbas, T. A. Tabish, S. J. Bull, T. M. Lim and A. N. Phan, *Sci. Rep.*, 2020, **10**, 21262.
105 E. Campbell, M. T. Hasan, R. Gonzalez Rodriguez, G. R. Akkaraju and A. V. Naumov, *ACS Biomater. Sci. Eng.*, 2019, **5**, 4671–4682.
106 W. Li, M. Li, Y. Liu, D. Pan, Z. Li, L. Wang and M. Wu, *ACS Appl. Nano Mater.*, 2018, **1**, 1623–1630.
107 M. K. Kumawat, M. Thakur, R. B. Gurung and R. Srivastava, *Sci. Rep.*, 2017, **7**, 15858.
108 B. Fresco-Cala, M. L. Soriano, A. Sciortino, M. Cannas, F. Messina and S. Cardenas, *RSC Adv.*, 2018, **8**, 29939–29946.
109 M. Yao, J. Huang, Z. Deng, W. Jin, Y. Yuan, J. Nie, H. Wang, F. Du and Y. Zhang, *Analyst*, 2020, **145**, 6981–6986.
110 H. Y. Nguyen, X. H. Le, N. T. Dao, N. T. Pham, T. H. H. Vu, N. H. Nguyen and T. N. Pham, *Adv. Nat. Sci.: Nanosci. Nanotechnol.*, 2019, **10**, 025005.
111 M. Zhang, L. Bai, W. Shang, W. Xie, H. Ma, Y. Fu, D. Fang, H. Sun, L. Fan, M. Han, C. Liu and S. Yang, *J. Mater. Chem.*, 2012, **22**, 7461–7467.
112 T. N. Lin, K. H. Chih, C. T. Yuan, J. L. Shen, C. A. J. Lin and W. R. Liu, *Nanoscale*, 2015, **7**, 2708–2715.
113 M. T. Hasan, R. Gonzalez-Rodriguez, C. Ryan, N. Faerber, J. L. Coffer and A. V. Naumov, *Adv. Funct. Mater.*, 2018, **28**, 1804337.
114 L.-L. Li, J. Ji, R. Fei, C.-Z. Wang, Q. Lu, J.-R. Zhang, L.-P. Jiang and J.-J. Zhu, *Adv. Funct. Mater.*, 2012, **22**, 2971–2979.
115 J. Peng, W. Gao, B. K. Gupta, Z. Liu, R. Romero-Aburto, L. Ge, L. Song, L. B. Alemany, X. Zhan, G. Gao, S. A. Vithayathil, B. A. Kaipparettu, A. A. Marti, T. Hayashi, J.-J. Zhu and P. M. Ajayan, *Nano Lett.*, 2012, **12**, 844–849.
116 X. Tan, Y. Li, X. Li, S. Zhou, L. Fan and S. Yang, *Chem. Commun.*, 2015, **51**, 2544–2546.
117 J. Shen, Y. Zhu, X. Yang and C. Li, *Chem. Commun.*, 2012, **48**, 3686–3699.
118 J. Shen, Y. Zhu, X. Yang, J. Zong, J. Zhang and C. Li, *New J. Chem.*, 2012, **36**, 97–101.
119 H. Li, X. He, Z. Kang, H. Huang, Y. Liu, J. Liu, S. Lian, C. H. Tsang, X. Yang and S. T. Lee, *Angew. Chem., Int. Ed*, 2010, **49**, 4430–4434.
120 G. Eda, Y. Y. Lin, C. Mattevi, H. Yamaguchi, H. A. Chen, I. S. Chen, C. W. Chen and M. Chhowalla, *Adv. Mater.*, 2010, **22**, 505–509.
121 J. Shen, Y. Zhu, C. Chen, X. Yang and C. Li, *Chem. Commun.*, 2011, **47**, 2580–2582.
122 T. Gokus, R. R. Nair, A. Bonetti, M. Böhmler, A. Lombardo, K. S. Novoselov, A. K. Geim, A. C. Ferrari and A. Hartschuh, *ACS Nano*, 2009, **3**, 3963–3968.
123 S. Zhuo, M. Shao and S.-T. Lee, *ACS Nano*, 2012, **6**, 1059–1064.
124 H. Li, X. He, Z. Kang, H. Huang, Y. Liu, J. Liu, S. Lian, C. H. A. Tsang, X. Yang and S.-T. Lee, *Angew. Chem., Int. Ed.*, 2010, **49**, 4430–4434.
125 S.-H. Choi, *J. Phys. D: Appl. Phys.*, 2017, **50**, 103002.
126 S. Campuzano, P. Yáñez-Sedeño and J. M. Pingarrón, *Nanomaterials*, 2019, **9**, 634.
127 T. Hu, L. Zhang, W. Wen, X. Zhang and S. Wang, *Biosens. Bioelectron.*, 2016, **77**, 451–456.
128 M. Pedrero, S. Campuzano and J. M. Pingarrón, *J. AOAC Int.*, 2017, **100**, 950–961.
129 M. Terrones, A. R. Botello-Méndez, J. Campos-Delgado, F. López-Urías, Y. I. Vega-Cantú, F. J. Rodríguez-Macías, A. L. Elías, E. Muñoz-Sandoval, A. G. Cano-Márquez, J.-C. Charlier and H. Terrones, *Nano Today*, 2010, **5**, 351–372.
130 T. Van Tam, S. G. Kang, K. F. Babu, E.-S. Oh, S. G. Lee and W. M. Choi, *J. Mater. Chem. A*, 2017, **5**, 10537–10543.
131 S. Yang, J. Sun, P. He, X. Deng, Z. Wang, C. Hu, G. Ding and X. Xie, *Chem. Mater.*, 2015, **27**, 2004–2011.

132 Y. Zhang, Q. Rong, J. Zhao, J. Zhang, Z. Zhu and Q. Liu, *J. Mater. Chem. A*, 2018, **6**, 12647–12653.
133 P. Wu, P. Du, H. Zhang and C. Cai, *Phys. Chem. Chem. Phys.*, 2013, **15**, 6920–6928.
134 X. Hou, Y. Li and C. Zhao, *Aust. J. Chem.*, 2016, **69**, 357–360.
135 Y. Li, Y. Zhao, H. Cheng, Y. Hu, G. Shi, L. Dai and L. Qu, *J. Am. Chem. Soc.*, 2012, **134**, 15–18.
136 D. Qu, M. Zheng, L. Zhang, H. Zhao, Z. Xie, X. Jing, R. E. Haddad, H. Fan and Z. Sun, *Sci. Rep.*, 2014, **4**, 5294.
137 M. Kaur, M. Kaur and V. K. Sharma, *Adv. Colloid Interface Sci.*, 2018, **259**, 44–64.
138 H. Shah, W. Xie, Y. Wang, X. Jia, A. Nawaz, Q. Xin, M. Song and J. R. Gong, *Mater. Sci. Eng.*, 2021, **119**, 111642.
139 A. O. Alqarni, S. A. Alkahtani, A. M. Mahmoud and M. M. El-Wekil, *Spectrochim. Acta, Part A*, 2021, **248**, 119180.
140 E. Budak and C. Ünlü, *Opt. Mater.*, 2021, **111**, 110577.
141 S. Gu, C.-T. Hsieh, C.-P. Kao, C.-C. Fu, Y. Ashraf Gandomi, R.-S. Juang and K. D. Kihm, *Catalysts*, 2021, **11**, 101.
142 L. Zhang, Z.-Y. Zhang, R.-P. Liang, Y.-H. Li and J.-D. Qiu, *Anal. Chem.*, 2014, **86**, 4423–4430.
143 S. Li, Y. Li, J. Cao, J. Zhu, L. Fan and X. Li, *Anal. Chem.*, 2014, **86**, 10201–10207.
144 N. Atar and M. L. Yola, *Anal. Chim. Acta*, 2021, **1148**, 338202.
145 K. Jlassi, S. Mallick, A. Eribi, M. M. Chehimi, Z. Ahmad, F. Touati and I. Krupa, *Sens. Actuators, B*, 2021, **328**, 129058.
146 S. Sangam, A. Gupta, A. Shakeel, R. Bhattacharya, A. K. Sharma, D. Suhag, S. Chakrabarti, S. K. Garg, S. Chattopadhyay, B. Basu, V. Kumar, S. K. Rajput, M. K. Dutta and M. Mukherjee, *Green Chem.*, 2018, **20**, 4245–4259.
147 R. V. Nair, R. T. Thomas, A. P. Mohamed and S. Pillai, *Microchem. J.*, 2020, **157**, 104971.
148 T. K. Mondal, D. Dinda and S. K. Saha, *Sens. Actuators, B*, 2018, **257**, 586–593.
149 W. Wang, S. Xu, N. Li, Z. Huang, B. Su and X. Chen, *Spectrochim. Acta, Part A*, 2019, **221**, 117211.
150 A. M. Bayoumy, A. Refaat, I. S. Yahia, H. Y. Zahran, H. Elhaes, M. A. Ibrahim and M. Shkir, *Opt. Quantum Electron.*, 2019, **52**, 16.
151 Z. Qian, J. Ma, X. Shan, L. Shao, J. Zhou, J. Chen and H. Feng, *RSC Adv.*, 2013, **3**, 14571–14579.
152 H. Sun, N. Gao, L. Wu, J. Ren, W. Wei and X. Qu, *Chem. – Eur. J.*, 2013, **19**, 13362–13368.
153 H. Tetsuka, R. Asahi, A. Nagoya, K. Okamoto, I. Tajima, R. Ohta and A. Okamoto, *Adv. Mater.*, 2012, **24**, 5333–5338.
154 R. Wang, H. Fan, W. Jiang, G. Ni and S. Qu, *Appl. Surf. Sci.*, 2019, **467-468**, 446–455.
155 T. V. Tam and W. M. Choi, *Curr. Appl. Phys.*, 2018, **18**, 1255–1260.
156 S. H. Jin, D. H. Kim, G. H. Jun, S. H. Hong and S. Jeon, *ACS Nano*, 2013, **7**, 1239–1245.
157 Z. Wang, J. Xia, C. Zhou, B. Via, Y. Xia, F. Zhang, Y. Li, L. Xia and J. Tang, *Colloids Surf., B*, 2013, **112**, 192–196.
158 Y. Lou, J. Ji, A. Qin, L. Liao, Z. Li, S. Chen, K. Zhang and J. Ou, *ACS Omega*, 2020, **5**, 6763–6772.
159 L. Wang, W. Li, B. Wu, Z. Li, S. Wang, Y. Liu, D. Pan and M. Wu, *Chem. Eng. J.*, 2016, **300**, 75–82.
160 O. J. Achadu, I. Uddin and T. Nyokong, *J. Photochem. Photobiol., A*, 2016, **324**, 96–105.
161 K. Li, J. Chen, Y. Yan, Y. Min, H. Li, F. Xi, J. Liu and P. Chen, *Carbon*, 2018, **136**, 224–233.
162 A. Dutta Chowdhury and R.-A. Doong, *ACS Appl. Mater. Interfaces*, 2016, **8**, 21002–21010.
163 R. Li, X. Wang, Z. Li, H. Zhu and J. Liu, *New J. Chem.*, 2018, **42**, 4352–4360.
164 N. Abdullah, Al, J.-E. Lee, I. In, H. Lee, K. D. Lee, J. H. Jeong and S. Y. Park, *Mol. Pharmaceutics*, 2013, **10**, 3736–3744.
165 R. Li, X. Wang, Z. Li, H. Zhu and J. Liu, *New J. Chem.*, 2018, **42**, 4352–4360.
166 S. Kadian, G. Manik, N. Das and P. Roy, *Microchim. Acta*, 2020, **187**, 458.
167 Y. He, X. Wang, J. Sun, S. Jiao, H. Chen, F. Gao and L. Wang, *Anal. Chim. Acta*, 2014, **810**, 71–78.
168 S. Arunragsa, Y. Seekaew, W. Pon-On and C. Wongchoosuk, *Diamond Relat. Mater.*, 2020, **105**, 107790.
169 R. Guo, S. Zhou, Y. Li, X. Li, L. Fan and N. H. Voelcker, *ACS Appl. Mater. Interfaces*, 2015, **7**, 23958–23966.
170 M. Park, Y. Jeong, H. S. Kim, W. Lee, S.-H. Nam, S. Lee, H. Yoon, J. Kim, S. Yoo and S. Jeon, *Adv. Funct. Mater.*, 2021, 2102741.
171 P.-Y. Lo, G.-Y. Lee, J.-H. Zheng, J.-H. Huang, E.-C. Cho and K.-C. Lee, *ACS Appl. Bio Mater.*, 2020, **3**, 5948–5956.
172 S. Kadian and G. Manik, *Food Chem.*, 2020, **317**, 126457.
173 T. Vats, S. Kumar and K. Jain, *Colloid Polym. Sci.*, 2014, **292**, 3025–3031.
174 N. Li, R. Li, Z. Li, Y. Yang, G. Wang and Z. Gu, *Sens. Actuators, B*, 2019, **283**, 666–676.
175 H. A. Kermani, M. Hosseini, M. Dadmehr, S. Hosseinkhani and M. R. Ganjali, *Sens. Actuators, B*, 2017, **241**, 217–223.
176 S. R. Ahmed, S. Kumar, G. A. Ortega, S. Srinivasan and A. R. Rajabzadeh, *Food Chem.*, 2021, **346**, 128893.
177 L. Ruiyi, J. Yanhong, W. Qinsheng, Y. Yongqiang, L. Nana, S. Xiulan and L. Zaijun, *Sens. Actuators, B*, 2021, **343**, 130099.
178 M. Masteri-Farahani, F. Ghorbani and N. Mosleh, *Spectrochim. Acta, Part A*, 2021, **245**, 118892.
179 L. Sun, S. Li, W. Ding, Y. Yao, X. Yang and C. Yao, *J. Mater. Chem. B*, 2017, **5**, 9006–9014.
180 J. Ryu, E. Lee, K. Lee and J. Jang, *J. Mater. Chem. B*, 2015, **3**, 4865–4870.
181 X. Li, S. Zhu, B. Xu, K. Ma, J. Zhang, B. Yang and W. Tian, *Nanoscale*, 2013, **5**, 7776–7779.
182 H. Liu, W. Na, Z. Liu, X. Chen and X. Su, *Biosens. Bioelectron.*, 2017, **92**, 229–233.
183 W. Na, N. Li and S. Xingguang, *Sens. Actuators, B*, 2018, **274**, 172–179.
184 N. Kongsanan, N. Pimsin, C. Keawprom, P. Sricharoen, Y. Areerob, P. Nuengmatcha, W.-C. Oh, S. Chanthai and N. Limchoowong, *ACS Omega*, 2021, **6**, 14379–14393.

185 B. Wang, J. Shen, Y. Huang, Z. Liu and H. Zhuang, *Int. J. Mol. Sci.*, 2018, **19**, 1696.
186 Z. Qu, W. Na, Y. Nie and X. Su, *Anal. Chim. Acta*, 2018, **1039**, 74–81.
187 D. Wu, C. Qu, J. Wang, R. Yang and L. Qu, *Luminescence*, 2021, e4062.
188 C. Sahub, T. Tuntulani, T. Nhujak and B. Tomapatanaget, *Sens. Actuators, B*, 2018, **258**, 88–97.
189 A. Ananthanarayanan, X. Wang, P. Routh, B. Sana, S. Lim, D. H. Kim, K. H. Lim, J. Li and P. Chen, *Adv. Funct. Mater.*, 2014, **24**, 3021–3026.
190 S. Patra, E. Roy, R. Choudhary, A. Tiwari, R. Madhuri and P. K. Sharma, *Biosens. Bioelectron.*, 2017, **1**, 627–635.
191 M. Amjadi and R. Jalili, *RSC Adv.*, 2016, **6**, 86736–86743.
192 H. Chen, Q. Wang, Q. Shen, X. Liu, W. Li, Z. Nie and S. Yao, *Biosens. Bioelectron.*, 2017, **91**, 878–884.
193 J. Hassanzadeh and A. Khataee, *Talanta*, 2018, **178**, 992–1000.
194 I. Al-Ogaidi, H. Gou, Z. P. Aguilar, S. Guo, A. K. Melconian, A. K. A. Al-Kazaz, F. Meng and N. Wu, *Chem. Commun.*, 2014, **50**, 1344–1346.
195 Z. S. Qian, X. Y. Shan, L. J. Chai, J. J. Ma, J. R. Chen and H. Feng, *Biosens. Bioelectron.*, 2014, **60**, 64–70.
196 W. Na, Q. Liu, B. Sui, T. Hu and X. Su, *Talanta*, 2016, **161**, 469–475.
197 X. Yan, X.-E. Zhao, J. Sun, S. Zhu, C. Lei, R. Li, P. Gong, B. Ling, R. Wang and H. Wang, *Sens. Actuators, B*, 2018, **263**, 27–35.
198 J. Sun, F. Cui, R. Zhang, Z. Gao, J. Ji, Y. Ren, F. Pi, Y. Zhang and X. Sun, *Anal. Chem.*, 2018, **90**, 11538–11547.
199 J. Shi, C. Chan, Y. Pang, W. Ye, F. Tian, J. Lyu, Y. Zhang and M. Yang, *Biosens. Bioelectron.*, 2015, **67**, 595–600.
200 C.-Y. Poon, Q. Li, J. Zhang, Z. Li, C. Dong, A. W.-M. Lee, W.-H. Chan and H.-W. Li, *Anal. Chim. Acta*, 2016, **917**, 64–70.
201 M. Laurenti, M. Paez-Perez, M. Algarra, P. Alonso-Cristobal, E. Lopez-Cabarcos, D. Mendez-Gonzalez and J. Rubio-Retama, *ACS Appl. Mater. Interfaces*, 2016, **8**, 12644–12651.
202 Q. Wang, L. Li, X. Wang, C. Dong and S. Shuang, *Talanta*, 2020, **219**, 121180.
203 Z. Kamal, M. Zarei Ghobadi, S. M. Mohseni and H. Ghourchian, *Biosens. Bioelectron.*, 2021, **188**, 113334.
204 G. Xue, M. Zhiying, L. Xiuying, T. Lijun and L. Jianrong, *J. Fluoresc.*, 2020, **30**, 1463–1468.
205 B. Wang, J. Shen, Y. Huang, Z. Liu and H. Zhuang, *Int. J. Mol. Sci.*, 2018, **19**, 1696.
206 J. Sun, F. Cui, R. Zhang, Z. Gao, J. Ji, Y. Ren, F. Pi, Y. Zhang and X. Sun, *Anal. Chem.*, 2018, **90**, 11538–11547.
207 J. Lou, S. Liu, W. Tu and Z. Dai, *Anal. Chem.*, 2015, **87**, 1145–1151.
208 K. Tian, F. Nie, K. Luo, X. Zheng and J. Zheng, *J. Electroanal. Chem.*, 2017, **801**, 162–170.
209 S. Chen, X. Chen, L. Zhang, J. Gao and Q. Ma, *ACS Appl. Mater. Interfaces*, 2017, **9**, 5430–5436.
210 Q. Lu, W. Wei, Z. Zhou, Z. Zhou, Y. Zhang and S. Liu, *Analyst*, 2014, **139**, 2404–2410.
211 R.-P. Liang, W.-B. Qiu, H.-F. Zhao, C.-Y. Xiang and J.-D. Qiu, *Anal. Chim. Acta*, 2016, **904**, 58–64.
212 Y. Yan, Q. Liu, X. Dong, N. Hao, S. Chen, T. You, H. Mao and K. Wang, *Microchim. Acta*, 2016, **183**, 1591–1599.
213 G. Jie, Q. Zhou and G. Jie, *Talanta*, 2019, **194**, 658–663.
214 H. Chen, W. Li, Q. Wang, X. Jin, Z. Nie and S. Yao, *Electrochim. Acta*, 2016, **214**, 94–102.
215 D. Wu, Y. Liu, Y. Wang, L. Hu, H. Ma, G. Wang and Q. Wei, *Sci. Rep.*, 2016, **6**, 20511.
216 Y. Lu, X. Zhao, Y. Tian, Q. Guo, C. Li and G. Nie, *Microchem. J.*, 2020, **157**, 104959.
217 S. Yang, M. Chu, J. Du, Y. Li, T. Gai, X. Tan, B. Xia and S. Wang, *R. Soc. Open Sci.*, 2020, **7**, 191404.
218 P. Liu, H. Meng, Q. Han, G. Zhang, C. Wang, L. Song and Y. Fu, *Microchim. Acta*, 2021, **188**, 120.
219 J. Peng, Z. Zhao, M. Zheng, B. Su, X. Chen and X. Chen, *Sens. Actuators, B*, 2020, **304**, 127383.
220 S. Chen, X. Chen, L. Zhang, J. Gao and Q. Ma, *ACS Appl. Mater. Interfaces*, 2017, **9**, 5430–5436.
221 Y. Yan, Q. Liu, X. Dong, N. Hao, S. Chen, T. You, H. Mao and K. Wang, *Microchim. Acta*, 2016, **183**, 1591–1599.
222 D. Wu, Y. Liu, Y. Wang, L. Hu, H. Ma, G. Wang and Q. Wei, *Sci. Rep.*, 2016, **6**, 20511.
223 E. C. Rama and A. Costa-García, *Electroanalysis*, 2016, **28**, 1700–1715.
224 S. A. Lim and M. U. Ahmed, *RSC Adv.*, 2016, **6**, 24995–25014.
225 R. Pradhan, S. A. Raisa, P. Kumar, A. Kalkal, N. Kumar, G. Packirisamy and S. Manhas, *Biomed. Microdevices*, 2021, **23**, 9.
226 P. Allawadhi, V. Singh, A. Khurana, I. Khurana, S. Allwadhi, P. Kumar, A. K. Banothu, S. Thalugula, P. J. Barani, R. R. Naik and K. K. Bharani, *Sens. Int.*, 2021, 100101, DOI: 10.1016/j.sintl.2021.100101.
227 V. Singh, P. Allawadhi, A. Khurana, A. K. Banothu and K. K. Bharani, *Sens. Int.*, 2021, **2**, 100098.
228 I.-H. Cho, J. Lee, J. Kim, M.-S. Kang, J. K. Paik, S. Ku, H.-M. Cho, J. Irudayaraj and D.-H. Kim, *Sensors*, 2018, **18**, 207.
229 C.-F. Wang, X.-Y. Sun, M. Su, Y.-P. Wang and Y.-K. Lv, *Analyst*, 2020, **145**, 1550–1562.
230 R. Mohammad-Rezei and H. Razmi, *Sens. Lett.*, 2016, **14**, 685–691.
231 S. K. Tuteja, R. Chen, M. Kukkar, C. K. Song, R. Mutreja, S. Singh, A. K. Paul, H. Lee, K.-H. Kim and A. Deep, *Biosens. Bioelectron.*, 2016, **86**, 548–556.
232 I. Vasilescu, S. A. Eremia, M. Kusko, A. Radoi, E. Vasile and G.-L. Radu, *Biosens. Bioelectron.*, 2016, **75**, 232–237.
233 J. Xi, C. Xie, Y. Zhang, L. Wang, J. Xiao, X. Duan, J. Ren, F. Xiao and S. Wang, *ACS Appl. Mater. Interfaces*, 2016, **8**, 22563–22573.
234 A. Valipour and M. Roushani, *Biosens. Bioelectron.*, 2017, **89**, 946–951.
235 F. Shahdost-fard and M. Roushani, *Biosens. Bioelectron.*, 2017, **87**, 724–731.
236 Q. Huang, X. Lin, L. Tong and Q.-X. Tong, *ACS Sustainable Chem. Eng.*, 2020, **8**, 1644–1650.

237 J. Xi, C. Xie, Y. Zhang, L. Wang, J. Xiao, X. Duan, J. Ren, F. Xiao and S. Wang, *ACS Appl. Mater. Interfaces*, 2016, **8**, 22563–22573.
238 S. K. Arumugasamy, S. Govindaraju and K. Yun, *Appl. Surf. Sci.*, 2020, **508**, 145294.
239 J. L. Gogola, G. Martins, A. Gevaerd, L. Blanes, J. Cardoso, F. K. Marchini, C. E. Banks, M. F. Bergamini and L. H. Marcolino-Junior, *Anal. Chim. Acta*, 2021, **1166**, 338548.
240 J. Cai, B. Sun, X. Gou, Y. Gou, W. Li and F. Hu, *J. Electroanal. Chem.*, 2018, **816**, 123–131.
241 L. Lu, L. Zhou, J. Chen, F. Yan, J. Liu, X. Dong, F. Xi and P. Chen, *ACS Nano*, 2018, **12**, 12673–12681.
242 B. Sun, Y. Wang, D. Li, W. Li, X. Gou, Y. Gou and F. Hu, *Mater. Sci. Eng.*, 2020, **111**, 110797.
243 A. Soleimanian, B. Khalilzadeh, M. Mahdipour, A. R. Aref, A. Kalbasi, S. R. Bazaz, M. E. Warkiani, M. R. Rashidi and M. Mahdavi, *IEEE Sens. J.*, 2021, 1, DOI: 10.1109/JSEN.2021.3079224.
244 N. Özcan, C. Karaman, N. Atar, O. Karaman and M. L. Yola, *ECS J. Solid State Sci. Technol.*, 2020, **9**, 121010.
245 H. Bhardwaj, C. A. Marquette, P. Dutta, Rajesh and G. Sumana, *Anal. Bioanal. Chem.*, 2020, **412**, 7029–7041.
246 H. Mahmoudi-Moghaddam, S. Tajik and H. Beitollahi, *Microchem. J.*, 2019, **150**, 104085.
247 G. Ashraf, M. Asif, A. Aziz, A. Q. Dao, T. Zhang, T. Iftikhar, Q. Wang and H. Liu, *Nanoscale*, 2020, **12**, 9014–9023.
248 N. Arab, L. Fotouhi, A. Salis and P. S. Dorraji, *New J. Chem.*, 2020, **44**, 15742–15751.
249 K. Ghanbari, M. Roushani and A. Azadbakht, *Anal. Biochem.*, 2017, **534**, 64–69.
250 K. Ghanbari and M. Roushani, *Bioelectrochemistry*, 2018, **120**, 43–48.
251 P. K. Gupta, D. Chauhan, Z. H. Khan and P. R. Solanki, *ACS Appl. Nano Mater.*, 2020, **3**, 2506–2516.
252 Y. Yang, Q. Liu, Y. Liu, J. Cui, H. Liu, P. Wang, Y. Li, L. Chen, Z. Zhao and Y. Dong, *Biosens. Bioelectron.*, 2017, **90**, 31–38.
253 A. B. Ganganboina and R.-A. Doong, *Sci. Rep.*, 2019, **9**, 1–11.
254 P. Zhang, X. Zhao, Y. Ji, Z. Ouyang, X. Wen, J. Li, Z. Su and G. Wei, *J. Mater. Chem. B*, 2015, **3**, 2487–2496.
255 S. K. Tuteja, R. Chen, M. Kukkar, C. K. Song, R. Mutreja, S. Singh, A. K. Paul, H. Lee, K.-H. Kim, A. Deep and C. R. Suri, *Biosens. Bioelectron.*, 2016, **86**, 548–556.
256 I. Vasilescu, S. A. V. Eremia, M. Kusko, A. Radoi, E. Vasile and G.-L. Radu, *Biosens. Bioelectron.*, 2016, **75**, 232–237.
257 Y. Li, W. Zhang, L. Zhang, J. Li, Z. Su and G. Wei, *Adv. Mater. Interfaces*, 2017, **4**, 1600895.
258 A. B. Ganganboina and R.-A. Doong, *Sci. Rep.*, 2019, **9**, 7214.